

Deterministic Approximate EM algorithm

Application to the Riemann approximation EM and the tempered EM

Thomas Lartigue^{1,2} · Stanley Durrleman¹ · Stéphanie Allasonnière³

the date of receipt and acceptance should be inserted later

Abstract The Expectation Maximisation (EM) algorithm is widely used to optimise non-convex likelihood functions with latent variables. Many authors modified its simple design to fit more specific situations. For instance, the Expectation (E) step has been replaced by Monte Carlo (MC), Markov Chain Monte Carlo or tempered approximations... Most of the well-studied approximations belong to the stochastic class. By comparison, the literature is lacking when it comes to deterministic approximations. In this paper, we introduce a theoretical framework, with state-of-the-art convergence guarantees, for any deterministic approximation of the E step. We analyse theoretically and empirically several approximations that fit into this framework. First, for cases with intractable E steps, we introduce a deterministic alternative to the MC-EM, using Riemann sums. This method is easy to implement and does not require the tuning of hyper-parameters. Then, we consider the tempered approximation, borrowed from the Simulated Annealing optimisation technique and meant to improve the EM solution. We prove that the tempered EM verifies the convergence guarantees for a wide range of temperature profiles. We showcase empirically

how it is able to escape adversarial initialisations. Finally, we combine the Riemann and tempered approximations to accomplish both their purposes.

Keywords Expectation Maximisation algorithm · exponential family · approximation · Riemann sum · tempering · annealing

Mathematics Subject Classification (2010) 62F99 · 49N30

1 Introduction

The Expectation Maximisation (EM) algorithm was introduced by Dempster, Laird and Rubin (DLR, 1977) to maximise likelihood functions $g(\theta)$ defined from inherent latent variables z and that were non-convex and had intricate gradients and Hessians. The EM algorithm estimates θ in an iterative fashion, starting from a certain initial value θ_0 and where the new estimate θ_{n+1} at step $n+1$ is function the estimate θ_n from the previous step n . In addition to presenting the method, DLR provide convergence guarantees on the sequence of estimated parameters $\{\theta_n\}_n$, namely that it converges towards a critical point of the likelihood function as the step n of the procedure grows. Their flawed proof for this results was later corrected by Wu (1983), and more convergence guarantees were studied by Boyles (1983). Since some likelihood functions are too complex to apply DLR's raw version of the EM, authors of later works have proposed alternative versions, usually with new convergence guarantees. On the one hand, when the maximisation step (M step) is problematic, other optimisation methods such as coordinate descent (Wu, 1983) or gradient descent (Lange, 1995) have been proposed. On the other hand, several works introduce

Thomas Lartigue
thomas.lartigue@inria.fr
Present e-mail: thomas.lartigue@dzne.de

Stanley Durrleman
stanley.durrleman@inria.fr

Stéphanie Allasonnière
stephanie.allasonniere@parisdescartes.fr

¹ Aramis project-team, Inria Paris, France

² CMAP, CNRS, École polytechnique, I.P. Paris, France

³ Centre de Recherche des Cordeliers, Université de Paris, INSERM, Sorbonne Université, France

new versions of the algorithm where the expectation step (E step), which can also be intractable, is approximated. Most of them rely on Monte Carlo (MC) methods and Stochastic Approximations (SA) to estimate this expectation. Notable examples include the Stochastic Approximation EM (SAEM, [Delyon et al. 1999](#)), the Monte Carlo EM (MC-EM, [Wei and Tanner 1990](#)), the Markov Chain Monte Carlo EM (MCMC-EM, [Fort and Moulines 2003](#)), the MCMC-SAEM ([Kuhn and Lavielle, 2005](#); [Allasonnière et al., 2010](#)) and the Approximate SAEM ([Allasonnière and Chevallier, 2019](#)). Random approximation of the E step have also been used in the case where the data is too voluminous to allow a full E step computation. See for instance the Incremental EM ([Neal and Hinton, 1998](#); [Ng and McLachlan, 2003](#)), the Online EM ([Cappé and Moulines, 2009](#)) and more recently the stochastic EM with variance reduction (sEM-vr) ([Chen et al., 2018](#)), the fast Incremental EM (FIEM) ([Karimi et al., 2019](#)) and the Stochastic Path-Integrated Differential Estimator EM (SPIDER-EM) ([Fort et al., 2020](#)). Most of these variants come with their own theoretical convergence guarantees for the models of the exponential family. Recent works have also provided theoretical analysis of the EM algorithm outside of the exponential family, with locally strongly-concave log-likelihood function around the global maxima by [Balakrishnan et al. \(2017\)](#), our without such strong-concavity assumption by [Dwivedi et al. \(2018\)](#). The stochastically approximated EM algorithms constitute an extensive catalogue of methods. Indeed, there are many possible variants of MCMC samplers that can be considered, as well as the additional parameters, such as the “burn-in” period length and the gain decrease sequence, that have to be set. All these choices have an impact on the convergence of these “EM-like” algorithms and making the appropriate ones for each problem can be overwhelming, see [Booth and Hobert \(1999\)](#); [Levine and Casella \(2001\)](#); [Levine and Fan \(2004\)](#), among others, for discussions on tuning the MC-EM alone. On several cases, one might desire to dispose of a simpler method, possibly non-stochastic, and non-parametric to run an EM-like algorithm for models with no closed forms. However the literature is lacking in that regards. The Quasi-Monte Carlo EM, introduced by [Pan and Thompson \(1998\)](#), is a deterministic version of Monte Carlo EM, however theoretical guarantees are not provided. In that vein, [Jank \(2005\)](#) introduces the randomised Quasi-Monte Carlo EM, which is not deterministic, and does not have theoretical guarantees either.

In addition to intractable E steps, EM procedures also commonly face a second issue: their convergence, when guaranteed, can be towards any maximum. This the-

oretical remark has crucial numerical implications. Indeed, most of the time, convergence is reached towards a sub-optimal local maximum, usually very dependent on the initialisation. To tackle this issue and improve the solutions of the algorithm, other types of, usually deterministic, approximations of the E step have been proposed. One notable example is the tempering (or “annealing”) of the conditional probability function used in the E step. Instead of replacing an intractable problem by a tractable one, the tempering approximation is used to find better local maxima of the likelihood profile during the optimisation process, in the spirit of the Simulated Annealing of [Kirkpatrick et al. \(1983\)](#) and the Parallel Tempering (or Annealing MCMC) of [Swendsen and Wang \(1986\)](#); [Geyer and Thompson \(1995\)](#). The deterministic annealing EM was introduced by [Ueda and Nakano \(1998\)](#) with a decreasing temperature profile; another temperature profile was proposed by [Naim and Gildea \(2012\)](#). Contrary to most of the studies on stochastic approximations, these two works do not provide theoretical convergence guarantees for the proposed tempered methods. Which, as a consequence, does not provide insight on the choice of the temperature scheme. Moreover, the tempered methods do not allow the use of the EM in case of an intractable E step. In their tempered SAEM algorithm, [Allasonnière and Chevallier \(2019\)](#) combine the stochastic and tempering approximations, which allows the SAEM to run, even with an intractable E step, while benefiting from the improved optimisation properties brought by the tempering. In addition, theoretical convergence guarantees are provided. However, this method is once again stochastic and parametric.

Overall, most of the literature on approximated E steps focuses on stochastic approximations that estimate intractable conditional probability functions. The few purely deterministic approximations proposed, such as the tempered/annealed EM, are used for other purposes, improving the optimisation procedure, and lack convergence guarantees.

In this paper, we propose a new, unified class of EM algorithms with deterministic approximations of the E step. We prove that members of this class benefit from the state of the art theoretical convergence guarantees of [Wu \(1983\)](#); [Lange \(1995\)](#); [Delyon et al. \(1999\)](#), under mild regularity conditions on the approximation. Then, we provide examples of approximations that fall under this framework and have practical applications. First, for E steps without closed form, we propose to use Riemann sums to estimate the intractable normalising factor. This “Riemann approximation EM” is a deterministic, less parametric, alternative to the MC-EM and its variants. Second, we prove that the deter-

ministic annealed EM (or “tempered EM”) of [Ueda and Nakano \(1998\)](#) is a member of our general deterministic class as well. We prove that the convergence guarantees are achieved with almost no condition of the temperature scheme, justifying the use of a wider range of temperature profile than those proposed by [Ueda and Nakano \(1998\)](#) and [Naim and Gildea \(2012\)](#). Finally, since the Riemann and tempered approximations are two separate methods that fulfil very different practical purposes, we also propose to associate the two approximations in the “tempered Riemann approximation EM” when both their benefits are desired.

In Section 2, we introduce our general class of deterministic approximated versions of the EM algorithm and prove their convergence guarantees, for models of the exponential family. We discuss the “Riemann approximation EM” in Section 3, the “tempered EM” in Section 4, and their association, “tempered Riemann approximation EM”, in Section 5.

We demonstrate empirically that the Riemann EM converges properly on a model with and an intractable E step, and that adding the tempering to the Riemann approximation allows in addition to get away from the initialisation and recover the true parameters. On a tractable Gaussian Mixture Model, we compare the behaviours and performances of the tempered EM and the regular EM. In particular, we illustrate that the tempered EM is able to escape adversarial initialisations, and consistently reaches better values of the likelihood than the unmodified EM, in addition to better estimating the model parameters.

2 Deterministic Approximate EM algorithm and its convergence for the curved exponential family

2.1 Context and motivation

In this section, we propose a new class of deterministic EM algorithms with approximated E step. This class of algorithms is general and includes both methods that estimate intractable E steps as well as methods that strive to improve the algorithm’s solution. We prove that members of this class benefit from the same convergence guarantees that can be found in the state of the art references ([Wu, 1983](#); [Lange, 1995](#); [Delyon et al., 1999](#)) for the classical EM algorithm, and under similar model assumptions. The only condition on the approximated distribution being that it converges towards the real conditional probability distribution with a l_2 regularity. Like the authors of [Delyon et al. \(1999\)](#); [Fort and Moulines \(2003\)](#); [Allasonnière and Chevallier](#)

(2019), we work with probability density functions belonging to the curved exponential family. The specific properties of which are given in the hypothesis $M1$ of Theorem 1.

The general framework of the EM is the following: a random variable x follows a parametric probability distribution with probability density function (pdf) depending on a parameter $\theta \in \Theta \subset \mathbb{R}^l$. We observe independent and identically distributed (iid) realisations of the distribution: $(x^{(1)}, \dots, x^{(N)})$ and wish to maximise with respect to θ the resulting likelihood, which is noted $g(\theta)$. In the notations and the discourse, we mostly ignore x as a variable since the observations $(x^{(1)}, \dots, x^{(N)})$ are supposed fixed throughout the reasoning. In particular, the sample size $N < +\infty$ is finite and fixed throughout this paper. We are not considering the asymptotic case where $N \rightarrow +\infty$. We assume there exists a latent variable z informing the behaviour of the observed variable x such that $g(\theta)$ is the integral of the complete likelihood $h(z; \theta)$: $g(\theta) = \int_z h(z; \theta) \mu(dz)$, with μ the reference measure. The conditional density function of z is then $p_\theta(z) := h(z; \theta)/g(\theta)$. The foundation of the EM algorithm is that while $\ln g(\theta)$ is hard to maximise in θ , the functions $\theta \mapsto \ln h(z; \theta)$ and even $\theta \mapsto \mathbb{E}_z[\ln h(z; \theta)]$ are easier to work with because of the information added by the latent variable z (or its distribution). In practice however, the actual value of z is unknown and its distribution $p_\theta(z)$ dependent on θ . Hence, the EM was introduced by [Dempster et al. \(1977\)](#) as the two-stages procedure starting from an initial point θ_0 and iterated over the number of steps n :

(E) With the current parameter θ_n , calculate the conditional probability $p_{\theta_n}(z)$;

(M) To get θ_{n+1} , maximise in $\theta \in \Theta$ the function $\theta \mapsto \mathbb{E}_{z \sim p_{\theta_n}(z)}[\ln h(z; \theta)]$;

Which can be summarised as:

$$\theta_{n+1} := T(\theta_n) := \operatorname{argmax}_{\theta \in \Theta} \mathbb{E}_{z \sim p_{\theta_n}(z)}[\ln h(z; \theta)] . \quad (1)$$

Where we call T the point to point map in Θ corresponding to one EM step. We will not redo the basic theory of the exact EM here, but this procedure noticeably increase $g(\theta_n)$ at each new step n . However, as discussed in the introduction, in many cases, one may prefer to or need to use an approximation of $p_{\theta_n}(z)$ instead of the exact analytical value.

In the following, we consider a deterministic approximation of $p_\theta(z)$ noted $\tilde{p}_{\theta,n}(z)$ which depends on the current step n and on which we make no assumption at the moment. The resulting steps, defining the “Approximate EM”, can be written under the same form as (1):

$$\theta_{n+1} := F_n(\theta_n) := \operatorname{argmax}_{\theta \in \Theta} \mathbb{E}_{z \sim \tilde{p}_{\theta,n}(z)} [\ln h(z; \theta)] . \quad (2)$$

Where $\{F_n\}_{n \in \mathbb{N}}$ is the sequence of point to point maps in Θ associated with the sequence of approximations $\{\tilde{p}_{\theta,n}(z)\}_{\theta \in \Theta; n \in \mathbb{N}}$. In order to ensure the desired convergence guarantees, we add a slight modification to this EM sequence: *re-initialisation of the EM sequence onto increasing compact sets*. This modification was introduced by [Chen et al. \(1987\)](#) and adapted by [Fort and Moulines \(2003\)](#). Assume that you dispose of an increasing sequence of compacts $\{K_n\}_{n \in \mathbb{N}}$ such that $\bigcup_{n \in \mathbb{N}} K_n = \Theta$ and $\theta_0 \in K_0$. Define $j_0 := 0$. Then, the transition $\theta_{n+1} = F_n(\theta_n)$ is accepted only if $F_n(\theta_n)$ belongs to the current compact K_{j_n} , otherwise the sequence is reinitialised at θ_0 . The idea behind this technique was originally introduced by . The steps of the resulting algorithm, called “Stable Approximate EM”, can be written as:

$$\begin{cases} \text{if } F_n(\theta_n) \in K_{j_n}, \text{ then } \theta_{n+1} = F_n(\theta_n), \text{ and } j_{n+1} := j_n \\ \text{if } F_n(\theta_n) \notin K_{j_n}, \text{ then } \theta_{n+1} = \theta_0, \text{ and } j_{n+1} := j_n + 1. \end{cases} \quad (3)$$

This re-initialisation of the EM sequence may seem like a hurdle, however, this truncation is mostly a theoretical requirement. In practice, the first compact K_0 is taken so large that it covers the most probable areas of Θ and the algorithms (2) and (3) are identical as long as the sequence $\{\theta_n\}_n$ does not diverges towards the border of Θ .

2.2 Theorem

In the following, we will state the convergence Theorem of Eq. (3) and provide a brief description of the main steps of the proof.

Theorem 1 (Convergence of the Stable Approximate EM) *Let $\{\theta_n\}_{n \in \mathbb{N}}$ be a sequence of the Stable Approximate EM defined in Eq. (3). Let us assume two sets of hypotheses:*

- **The M1 – 3 conditions of Fort and Moulines (2003).**

M1. $\Theta \subseteq \mathbb{R}^l$, $\mathcal{X} \subseteq \mathbb{R}^d$ and μ is a σ -finite positive Borel measure on \mathcal{X} . Let $\psi : \Theta \rightarrow \mathbb{R}$, $\phi : \Theta \rightarrow \mathbb{R}^q$ and $S : \mathcal{X} \rightarrow \mathcal{S} \subseteq \mathbb{R}^q$. Define $L : \mathcal{S} \times \Theta \rightarrow \mathbb{R}$ and $h : \mathcal{X} \times \Theta \rightarrow \mathbb{R}_+ \setminus \{0\}$:

$$L(s; \theta) := \psi(\theta) + \langle s, \phi(\theta) \rangle, \quad h(z; \theta) := \exp(L(S(z); \theta)) .$$

M2. Assume that

(a*) ψ and ϕ are continuous on Θ ;

(b) for all $\theta \in \Theta$, $\bar{S}(\theta) := \int_{\mathcal{S}} S(z) p_{\theta}(z) \mu(dz)$ is finite and continuous on Θ ;

(c) there exists a continuous function $\hat{\theta} : \mathcal{S} \rightarrow \Theta$ such that for all $s \in \mathcal{S}$, $L(s; \hat{\theta}(s)) = \sup_{\theta \in \Theta} L(s; \theta)$;

(d) g is positive, finite and continuous on Θ and the level set $\{\theta \in \Theta, g(\theta) \geq M\}$ is compact for any $M > 0$.

M3. Assume either that:

(a) The set $g(\mathcal{L})$ is compact or

(a') for all compact sets $K \subseteq \Theta$, $g(K \cap \mathcal{L})$ is finite.

- **The conditions on the approximation.** Assume that $\tilde{p}_{\theta,n}(z)$ is deterministic. Let $S(z) = \{S_u(z)\}_{u=1}^q$. For all indices u , for any compact set $K \subseteq \Theta$, one of the two following configurations holds:

$$\begin{cases} \int_{\mathcal{S}} S_u^2(z) dz < \infty, \\ \sup_{\theta \in K} \int_{\mathcal{S}} (\tilde{p}_{\theta,n}(z) - p_{\theta}(z))^2 dz \xrightarrow{n \infty} 0. \end{cases} \quad (4)$$

Or

$$\begin{cases} \sup_{\theta \in K} \int_{\mathcal{S}} S_u^2(z) p_{\theta}(z) dz < \infty, \\ \sup_{\theta \in K} \int_{\mathcal{S}} \left(\frac{\tilde{p}_{\theta,n}(z)}{p_{\theta}(z)} - 1 \right)^2 p_{\theta}(z) dz \xrightarrow{n \infty} 0. \end{cases} \quad (5)$$

Then,

- (i) (a) $\lim_{n \infty} j_n < \infty$ and $\sup_{n \in \mathbb{N}} \|\theta_n\| < \infty$, with probability 1;
- (b) $g(\theta_n)$ converges towards a connected component of $g(\mathcal{L})$.
- (ii) If, additionally, $g(\mathcal{L} \cap \text{Cl}(\{\theta_n\}_{n \in \mathbb{N}}))$ has an empty interior, then:

$$g(\theta_n) \xrightarrow{n \infty} g^*,$$

$$d(\theta_n, \mathcal{L}_{g^*}) \xrightarrow{n \infty} 0.$$

With $\mathcal{L} := \{\theta \in \Theta | \nabla g(\theta) = 0\}$ and $\mathcal{L}_{g^*} := \{\theta \in \mathcal{L} | g(\theta) = g^*\}$.

Remark 1 – M2 (a) is modified with regards to [Fort and Moulines \(2003\)](#), we remove the hypothesis that S has to be a continuous function of z that is not needed when the approximation is not stochastic. We call M2 (a*) this new sub-hypothesis.

- The condition $\int_{\mathcal{S}} S_u^2(z) dz < \infty$ of the condition (4) can seem hard to verify since S is not integrated against a probability function. However, when z is a finite variable, as is the case for finite mixtures, this integral becomes a finite sum.
- The two sufficient conditions (4) and (5) involve a certain form of L^2 convergence of $\tilde{p}_{\theta,n}$ towards p_{θ} . If the latent variable z is continuous, this excludes countable (and finite) approximations such as sums

of Dirac functions, since they have a measure of zero. In particular, this excludes Quasi-Monte Carlo approximations. However, one look at the proof of Theorem 1 (in supplementary materials) or at the following sketch of proof reveals that verifying the convergence $\sup_{\theta \in K} \|\tilde{S}_n(\theta) - \tilde{S}(\theta)\| \xrightarrow{n \rightarrow \infty} 0$ for any compact set K is actually a sufficient condition to benefit from the results of Theorem 1. This condition can be verified by finite approximations.

2.3 Sketch of proof

The detailed proof of this results can be found in supplementary materials, we propose here a abbreviated version where we highlight the key steps.

Two intermediary propositions, introduced and proven in Fort and Moulines (2003), are instrumental in the proof of Theorem 1. These two propositions are called Propositions 9 and 11 by Fort and Moulines, and used to prove their Theorem 3. In our case, with the new condition $M2(a^*)$ and the absence of Monte Carlo sum, the reasoning for verifying the conditions of applicability of the two proposition is quite different from Fort and Moulines (2003) and will be highlighted below. First, let us state these two propositions:

Proposition 1 (“Proposition 9”) *Let $\Theta \subseteq \mathbb{R}^l$, K compact $\subset \Theta$, $\mathcal{L} \subseteq \Theta$ such that $\mathcal{L} \cap K$ compact. Let us assume*

- WC^0 Lyapunov function with regards to (T, \mathcal{L}) .
- $\exists u_n \in K^{\mathbb{N}}$ such that $|W(u_{n+1}) - W \circ T(u_n)| \xrightarrow{n \rightarrow \infty} 0$

Then

- $\{W(u_n)\}_{n \in \mathbb{N}}$ converges towards a connected component of $W(\mathcal{L} \cap K)$
- If $W(\mathcal{L} \cap K)$ has an empty interior, then $\{W(u_n)\}_n$ converges towards w^* and $\{u_n\}_n$ converges towards the set $\mathcal{L}_{w^*} \cap K$

Where $\mathcal{L}_{w^*} := \{\theta \in \mathcal{L} | W(\theta) = w^*\}$.

Proposition 2 (“Proposition 11”) *Let $\Theta \subseteq \mathbb{R}^l$, T and $\{F_n\}_n$ point to point maps on Θ . Let $\{\theta_n\}_n$ be the sequence defined by the Stable Approximate EM with likelihood g and approximate maps sequence $\{F_n\}_n$. Let $\mathcal{L} \subset \Theta$. We assume*

- the A1 – 2 conditions of Proposition 10 of Fort and Moulines (2003).
- (A1) There exists W , a C^0 Lyapunov function with regards to (T, \mathcal{L}) such that for all $M > 0$, $\{\theta \in \Theta, W(\theta) > M\}$ is compact, and:

$$\Theta = \bigcup_{n \in \mathbb{N}} \{\theta \in \Theta | W(\theta) > n^{-1}\}.$$

- (A2) $W(\mathcal{L})$ is compact OR (A2’) $W(\mathcal{L} \cap K)$ is finite for all compact $K \subseteq \Theta$.
- $\forall u \in K_0, \lim_{n \rightarrow \infty} |W \circ F_n - W \circ T|(u) = 0$
- \forall compact $K \subseteq \Theta$:

$$\lim_{n \rightarrow \infty} |W \circ F_n(u_n) - W \circ T(u_n)| \mathbb{1}_{u_n \in K} = 0$$

Then:

With probability 1, $\limsup_{n \rightarrow \infty} j_n < \infty$ and $\{u_n\}_n$ is a compact sequence.

For the proofs of these two results, see Fort and Moulines (2003). The proof of Theorem 1 is structured as follows: verifying the conditions of Proposition 2, applying Proposition 2, verifying the conditions of Proposition 1 and finally applying Proposition 1.

Verifying the conditions of Proposition 2. We first make explicit which object of our model plays which part in the Proposition. Let g be the likelihood function of a model of the curved exponential family.

- The set of its critical points is called \mathcal{L} :

$$\mathcal{L} := \{\theta \in \Theta | \nabla g(\theta) = 0\}.$$

- We call T the point to point map describing the transition between θ_n and θ_{n+1} in the exact EM algorithm, that is to say $T := \theta \circ \tilde{S}$.
- The general properties of the EM tell us that its stationary points are the critical points of g : $\mathcal{L} = \{\theta \in \Theta | T(\theta) = \theta\}$. Additionally, we have that g is a C^0 Lyapunov function associated to (T, \mathcal{L}) , hence it is fit to play the part of W from Proposition 2.
- Let $\{\theta_n\}_n$ be the sequence defined by the Stable Approximate EM, and $\{F_n\}_n$ the corresponding sequence of point to point maps.

With this setup, the assumptions M1 – 3 of Theorem 1 directly imply that A1 and A2 or A2’ are verified.

We need to prove that the last two conditions for Proposition 2 are verified:

$$\forall \theta \in K_0, \lim_{n \rightarrow \infty} |g \circ F_n - g \circ T|(\theta) = 0, \quad (6)$$

$$\forall \text{compact } K \subseteq \Theta, \lim_{n \rightarrow \infty} |g \circ F_n(\theta_n) - g \circ T(\theta_n)| \mathbb{1}_{\theta_n \in K} = 0. \quad (7)$$

At this stage, the steps to prove these two conditions differ from Fort and Moulines (2003). We denote $\tilde{S}_n(\theta_n)$ the approximated E step in the Stable Approximate

EM (so that $F_n = \hat{\theta} \circ \tilde{S}_n$). By using uniform continuity properties on compacts, we first obtain that

$$\forall \text{ compact } K, \sup_{\theta \in K} \|\tilde{S}_n(\theta) - \bar{S}(\theta)\| \xrightarrow{n \rightarrow \infty} 0, \quad (8)$$

is a sufficient condition to obtain both (6) and (7), and conclude that we can apply Proposition 2. Writing \tilde{S}_n and \bar{S} as integrals in z makes it clear that the two hypothesis (4) and (5) of Theorem 1 are both sufficient to have (8). Which concludes this section of the Proof.

Applying Proposition 2. Since we verify all the condition of Proposition 2, we can apply its conclusion. With probability 1:

$\limsup_{n \rightarrow \infty} j_n < \infty$ and $\{\theta_n\}_n$ is a compact sequence.

Which is specifically the result (i)(a) of Theorem 1.

Verifying the conditions of Proposition 1. With Proposition 1, we prove the remaining points of Theorem 1: (i)(b) and (ii).

For the application of Proposition 1:

- $Cl(\{\theta_n\}_n)$ plays the part of the compact K
- $\{\theta \in \Theta | \nabla g(\theta) = 0\} = \{\theta \in \Theta | T(\theta) = \theta\}$ plays the part of the set \mathcal{L}
- The likelihood g is the C^0 Lyapunov function with regards to (T, \mathcal{L})
- $\{\theta_n\}_n$ is the K valued sequence (as K is $Cl(\{\theta_n\}_n)$).

The last condition that remains to be shown to apply Proposition 1 is that:

$$\lim_{n \rightarrow \infty} |g(\theta_{n+1}) - g \circ T(\theta_n)| = 0.$$

In our previous efforts to prove (6) and (7), we have more or less already proven that with $F_n(\theta_n)$ in place of θ_{n+1} . The only indices where $F_n(\theta_n) \neq \theta_{n+1}$ are when the value of the sequence j_n experiences an increment of 1.

$$\begin{aligned} |g(\theta_{n+1}) - g \circ T(\theta_n)| &= |g(\theta_0) - g \circ T(\theta_n)| \mathbb{1}_{j_{n+1}=j_n+1} \\ &\quad + |g \circ F_n(\theta_n) - g \circ T(\theta_n)| \mathbb{1}_{j_{n+1}=j_n}. \end{aligned}$$

We have proven with Proposition 2 that there is only a finite number of such increments and that $Cl(\{\theta_k\}_k)$ is a compact. Since θ_n is always in $Cl(\{\theta_k\}_k)$ by definition, we can apply to $K := Cl(\{\theta_k\}_k)$ the result:

$$\forall \text{ compact } K \subseteq \Theta, \lim_{n \rightarrow \infty} |g \circ F_n(\theta_n) - g \circ T(\theta_n)| \mathbb{1}_{\theta_n \in K} = 0,$$

that we proved in order to verify Proposition 2, and get the needed condition:

$$\lim_{n \rightarrow \infty} |g(\theta_{n+1}) - g \circ T(\theta_n)| = 0.$$

Applying Proposition 1 Since we verify all we need to apply the conclusions of Proposition 1:

- $\{g(\theta_n)\}_{n \in \mathbb{N}}$ converges towards a connected component of $g(\mathcal{L} \cap Cl(\{\theta_n\}_n)) \subset g(\mathcal{L})$.
- If $g(\mathcal{L} \cap Cl(\{\theta_n\}_n))$ has an empty interior, then the sequence $\{g(\theta_n)\}_{n \in \mathbb{N}}$ converges towards a $g^* \in \mathbb{R}$ and $\{\theta_n\}_n$ converges towards $\mathcal{L}_{g^*} \cap Cl(\{\theta_n\}_n)$. Where $\mathcal{L}_{g^*} := \{\theta \in \mathcal{L} | g(\theta) = g^*\}$

Which are both respectively exactly (i)(b) and (ii) of Theorem 1 and concludes the proof of the Theorem.

3 Riemann approximation EM

3.1 Context and motivation

In this section, we introduce one specific case of Approximate EM useful in practice: approximating the conditional probability density function $p_\theta(z)$ at the E step by a Riemann sum, in the scenario where the latent variable z is continuous and bounded. We call this procedure the ‘‘Riemann approximation EM’’. After motivating this approach, we prove that it is an instance of the Approximate EM algorithm and verifies the hypotheses of Theorem 1, therefore benefits from the convergence guarantees.

When the conditional probability $p_\theta(z)$ is a continuous function, and even if $h(z; \theta)$ can be computed point by point, a closed form may not exist for the renormalisation term $g(\theta) = \int_z h(z; \theta) dz$. In that case, this integral is usually approximated stochastically with a Monte Carlo estimation, see for instance Delyon et al. (1999); Fort and Moulines (2003); Allasonnière and Chevalier (2019). When the dimension is reasonably small, a deterministic approximation through Riemann sums can also be performed. Unlike the stochastic methods, which often require to define and tune a Markov Chain, the Riemann approximation involves almost no parameter. The user only needs to choose the position of the Riemann intervals, a choice which is very guided by the well known theories of integration (Lagrange, Legendre...).

We introduce the Riemann approximation as a member of the Approximate EM class. Since z is supposed bounded in this section, without loss of generality, we will assume that z is a real variable and $z \in [0, 1]$. We recall that $p_\theta(z) = h(z; \theta)/g(\theta) = h(z; \theta)/\int_z h(z; \theta) dz$. Instead of using the exact joint likelihood $h(z; \theta)$, we define a sequence of step functions $\{\tilde{h}_n\}_{n \in \mathbb{N}^*}$ as: $\tilde{h}_n(z; \theta) := h(\lfloor \varphi(n)z \rfloor / \varphi(n); \theta)$. Where φ is an increasing function from $\mathbb{N}^* \rightarrow \mathbb{N}^*$ such that $\varphi(n) \xrightarrow{n \rightarrow \infty} \infty$. For the sake of simplicity, we will take $\varphi = Id$, hence $\tilde{h}_n(z; \theta) = h(\lfloor nz \rfloor / n; \theta)$. The following results, however, can be applied to any increasing function φ with $\varphi(n) \xrightarrow{n \rightarrow \infty} \infty$.

With these steps functions, the renormalising factor $\tilde{g}_n(\theta) := \int_z \tilde{h}_n(z; \theta) dz$ is now a finite sum. That is: $\tilde{g}_n(\theta) = \frac{1}{n} \sum_{k=0}^{n-1} h(\lfloor kz \rfloor / n; \theta)$. The approximate conditional probability $\tilde{p}_n(\theta)$ is then naturally defined as: $\tilde{p}_n(\theta) := \tilde{h}_n(z; \theta) / \tilde{g}_n(\theta)$. Thanks to the replacement of the integral by the finite sum, this deterministic approximation is much easier to compute than the real conditional probability.

3.2 Theorem and proof

We state and prove the following Theorem for the convergence of the EM with a Riemann approximation.

Theorem 2 *Under conditions M1 – 3 of Theorem 1, and when z is bounded, the (Stable) Approximate EM with $\tilde{p}_{n,\theta}(z) := \frac{h(\lfloor nz \rfloor / n; \theta)}{\int_z h(\lfloor nz' \rfloor / n; \theta) dz'}$, which we call “Riemann approximation EM”, verifies the remaining conditions of applicability of Theorem 1 as long as $z \mapsto S(z)$ is continuous.*

Proof This is the detailed proof of Theorem 2.

The conditions M1 – 3 on the model are already assumed to be verified. In order to apply Theorem 1, we need to verify either Eq. (4) or (5). Here, with $z \mapsto S(z)$ continuous, we prove Eq. (4): For any compact $K \subseteq \Theta$,

$$\begin{cases} \int_z S_u^2(z) dz < \infty \\ \sup_{\theta \in K} \int_z (\tilde{p}_{\theta,n}(z) - p_\theta(z))^2 dz \xrightarrow{n \rightarrow \infty} 0. \end{cases}$$

Since z is bounded (and assumed to be in $[0, 1]$ for simplicity) and S is continuous, the first part of the condition is easily verified: $\int_{z=0}^1 S_u^2(z) dz < \infty$. Only the second part remains to be proven.

First we note that $h(z; \theta) = \exp(\psi(\theta) + \langle S(z), \phi(\theta) \rangle)$ is continuous in (z, θ) , hence uniformly continuous on the compact set $[0, 1] \times K$. Additionally, we have:

$$\begin{aligned} 0 < m &:= \min_{(z, \theta) \in [0, 1] \times K} h(z; \theta) \leq h(z; \theta), \\ h(z; \theta) &\leq \max_{(z, \theta) \in [0, 1] \times K} h(z; \theta) =: M < \infty. \end{aligned}$$

Where m and M are constants independent of z and θ . This also means that $m \leq g(\theta) = \int_{z=0}^1 h(z; \theta) dz \leq M$. Moreover, since $\tilde{h}_n(z; \theta) = h(\lfloor nz \rfloor / n; \theta)$, then we also have $\forall z \in [0, 1], \theta \in K, n \in \mathbb{N}, m \leq \tilde{h}_n(z; \theta) \leq M$ and $m \leq \tilde{g}_n(\theta) = \int_{z=0}^1 \tilde{h}_n(z; \theta) dz \leq M$.

As h is uniformly continuous, $\forall \epsilon > 0, \exists \delta > 0, \forall (z, z') \in [0, 1]^2, (\theta, \theta') \in K^2$:

$$|z - z'| \leq \delta \text{ and } \|\theta - \theta'\| \leq \delta \Rightarrow |h(z; \theta) - h(z'; \theta')| \leq \epsilon.$$

By definition, $\lfloor nz \rfloor / n - z \leq 1/n$. Hence $\exists N \in \mathbb{N}, \forall n \geq N, \lfloor nz \rfloor / n - z \leq \delta$. As a consequence:

$$\forall \epsilon > 0, \exists N \in \mathbb{N}, \forall n \geq N, \forall (z, \theta) \in [0, 1] \times K, \quad |h(z; \theta) - \tilde{h}_n(z; \theta)| \leq \epsilon.$$

In other words, $\{\tilde{h}_n\}_n$ converges uniformly towards h . Let ϵ be given, we assume that $n \geq N$, then $\forall (z, \theta) \in [0, 1] \times K$:

$$\begin{aligned} \tilde{p}_{\theta,n}(z) - p_\theta(z) &= \frac{\tilde{h}_n(z; \theta)}{\int_z \tilde{h}_n(z; \theta) dz} - \frac{h(z; \theta)}{\int_z h(z; \theta) dz} \\ &= \frac{\tilde{h}_n(z; \theta) - h(z; \theta)}{\int_z \tilde{h}_n(z; \theta) dz} \\ &\quad + h(z; \theta) \frac{\int_z (h(z; \theta) - \tilde{h}_n(z; \theta)) dz}{\int_z h(z; \theta) dz \int_z \tilde{h}_n(z; \theta) dz} \\ &\leq \frac{\epsilon}{m} + M \frac{\epsilon}{m^2} \\ &= \epsilon \frac{m + M}{m^2}. \end{aligned}$$

Hence, $\forall n \geq N$:

$$\sup_{\theta \in K} \int_{z=0}^1 (\tilde{p}_{\theta,n}(z) - p_\theta(z))^2 dz \leq \epsilon^2 \left(\frac{m + M}{m^2} \right)^2.$$

Then, $\sup_{\theta \in K} \int_{z=0}^1 (\tilde{p}_{\theta,n}(z) - p_\theta(z))^2 dz \xrightarrow{n \rightarrow \infty} 0$, by definition. This was the last hypothesis needed to apply Theorem 1. Which concludes the proof.

3.3 Application to a Gaussian model with the Beta prior

We demonstrate the interest of the method on a example with a continuous bounded random variable following a Beta distribution $z \sim \text{Beta}(\alpha, 1)$, and an observed random variable following $x \sim \mathcal{N}(\lambda z, \sigma^2)$. In other words, with $\epsilon \sim \mathcal{N}(0, 1)$ independent of z :

$$x = \lambda z + \sigma \epsilon.$$

This results in a likelihood belonging to the exponential family:

$$h(z; \theta) = \frac{\alpha z^{\alpha-1}}{\sqrt{2\pi\sigma^2}} \exp\left(-\frac{(x - \lambda z)^2}{2\sigma^2}\right).$$

Since z is bounded, and everything is continuous in the parameter $(\alpha, \lambda, \sigma^2)$, this model easily verifies each of the conditions M1 – 3. The E step with this model involves the integral $\int_z z^\alpha \exp\left(-\frac{(x - \lambda z)^2}{2\sigma^2}\right) dz$, a fractional moment of the Gaussian distribution. Theoretical formulas exists for these moments, see Winkelbauer (2012),

however they involve Kummer's confluent hypergeometric functions, which are infinite series. Instead, we use the Riemann approximation to run the EM algorithm with this model: $\tilde{h}_n(z; \theta) := h(\lfloor \varphi(n)z \rfloor / \varphi(n); \theta)$. As done previously, we take, without loss of generality, $\varphi(n) := n$ for the sake of simplicity. The E step only involves the n different values taken by the step function probabilities $h(\lfloor nz \rfloor / n; \theta)$:

$$\tilde{p}_{\theta,n}^{(i)}\left(\frac{k}{n}\right) = \frac{h^{(i)}\left(\frac{k}{n}; \theta\right)}{\frac{1}{n} \sum_{l=0}^{n-1} h^{(i)}\left(\frac{l}{n}; \theta\right)}.$$

Where the exponent (i) indicates the index of the observation $x^{(i)}$. To express the corresponding M step in a digest way, let us define the operator $\Psi^{(i)} : \mathbb{R}^{[0,1]} \rightarrow \mathbb{R}$ such that, for any $f : [0, 1] \rightarrow \mathbb{R}$:

$$\Psi^{(i)} \circ f = \sum_{k=0}^{n-1} \tilde{p}_{\theta,n}^{(i)}\left(\frac{k}{n}\right) \int_{z=k/n}^{(k+1)/n} f(z) dz.$$

Then, the M step can be expressed as:

$$\begin{aligned} \frac{1}{\hat{\alpha}} &= -\frac{1}{N} \sum_{i=1}^N \Psi^{(i)} \circ \ln(z), \\ \hat{\lambda} &= \frac{\sum_{i=1}^N \Psi^{(i)} \circ (x^{(i)} z)}{\sum_{i=1}^N \Psi^{(i)} \circ z^2}, \\ \hat{\sigma}^2 &= \frac{1}{N} \sum_{i=1}^N \Psi^{(i)} \circ \left(x^{(i)} - \hat{\lambda} z\right)^2. \end{aligned} \quad (9)$$

Where we took the liberty of replacing f by $f(z)$ in these equations for the sake of simplicity. Here N is the total number of observations: $x := (x^{(1)}, \dots, x^{(N)})$ iid. We test this algorithm on synthetic data. With real values $\alpha = 2, \lambda = 5, \sigma = 1.5$, we generate a dataset with $N = 100$ observations and run the Riemann EM with random initialisation. This simulation is ran 2000 times. We observe that the Riemann EM is indeed able to increase the likelihood, despite the EM being originally intractable. On Fig. 1, we display the average trajectory, with standard deviation, of the negative log-likelihood $-\ln(g(\theta))$ during the Riemann EM procedure. The profile is indeed decreasing. The standard deviation around the average value is fairly high, since each run involves a different dataset and a different random initialisation, hence different value of the likelihood, but the decreasing trend is the same for all of the runs. We also display the average relative square errors on the parameters at the end of the algorithm. They are all small, with reasonably small standard deviation, which indicates that the algorithm consistently recovers correctly the parameters.

To evaluate the impact of the number of Riemann intervals $\varphi(n)$, we run a second experiment where we compare four different profiles over 50 simulations:

$$\begin{aligned} \text{(low)} \quad \varphi_1(n) &:= n + 1 \\ \text{(medium)} \quad \varphi_2(n) &:= n + 100 \\ \text{(high)} \quad \varphi_3(n) &:= n + 1000 \\ \text{(linear)} \quad \varphi_4(n) &:= 10 \times n + 1. \end{aligned}$$

The results are displayed on Fig. 2. We can see that, despite the very different profiles, the optimisations are very similar. The "low" profile performs slightly worst, which indicates that a high number of Riemann intervals is most desirable in practice. As long as this number is high enough, Fig. 2 suggests that the performances will not depend too much on the profile.

3.4 Application in two dimensions

The difficulty faced by Riemann methods in general is their geometric complexity when the dimension increases. In this section, we propose a similar experiment in two dimensions to show that the method is still functional and practical in that case.

For this 2D-model, we consider two latent independent Beta random variables $z_1 \sim \text{Beta}(\alpha_1, 1)$ and $z_2 \sim \text{Beta}(\alpha_2, 1)$, and two observed variables defined as:

$$\begin{aligned} x_1 &= \lambda_1 z_1 + z_2 + \sigma_1 \epsilon_1 \\ x_2 &= z_1 + \lambda_2 z_2 + \sigma_2 \epsilon_2, \end{aligned}$$

with $\epsilon_1 \sim \mathcal{N}(0, 1)$, $\epsilon_2 \sim \mathcal{N}(0, 1)$, and $(z_1, z_2, \epsilon_1, \epsilon_2)$ independent. The 2-dimension version of the Riemann E step with n intervals on each dimension is:

$$\tilde{p}_{\theta,n}^{(i)}\left(\frac{k_1}{n}, \frac{k_2}{n}\right) = \frac{h^{(i)}\left(\frac{k_1}{n}, \frac{k_2}{n}; \theta\right)}{\frac{1}{n^2} \sum_{l_1, l_2=0}^{n-1} h^{(i)}\left(\frac{l_1}{n}, \frac{l_2}{n}; \theta\right)}.$$

As before, we define an operator $\Psi^{(i)} : \mathbb{R}^{[0,1]^2} \rightarrow \mathbb{R}$ such that, for any $f : [0, 1]^2 \rightarrow \mathbb{R}$:

$$\Psi^{(i)} \circ f = \sum_{k_1, k_2=0}^{n-1} \tilde{p}_{\theta,n}^{(i)}\left(\frac{k_1}{n}, \frac{k_2}{n}\right) \int_{z_1, z_2=k/n}^{(k+1)/n} f(z_1, z_2) dz.$$

Then, the M step can be expressed as:

$$\begin{aligned} \frac{1}{\hat{\alpha}_1} &= -\frac{1}{N} \sum_{i=1}^N \Psi^{(i)} \circ \ln(z_1), \\ \hat{\lambda}_1 &= \frac{\sum_i \Psi^{(i)} \circ (x_1^{(i)} z_1 - z_2 z_1)}{\sum_i \Psi^{(i)} \circ z_1^2}, \\ \hat{\sigma}_1 &= \frac{1}{N} \sum_{i=1}^N \Psi^{(i)} \circ \left(x_1^{(i)} - \hat{\lambda}_1 z_1 - z_2\right)^2, \end{aligned}$$

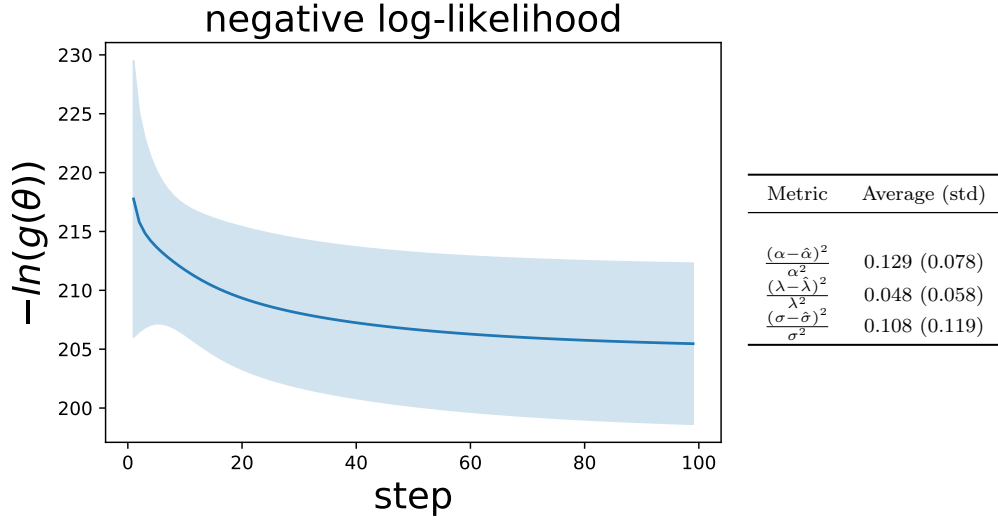


Fig. 1 (Right). Average values, with standard deviation, over 2000 simulations of the negative log-likelihood along the steps of the Riemann EM. The Riemann EM increases the likelihood. (Left). Average and standard deviation of the relative parameter reconstruction errors at the end of the Riemann EM.

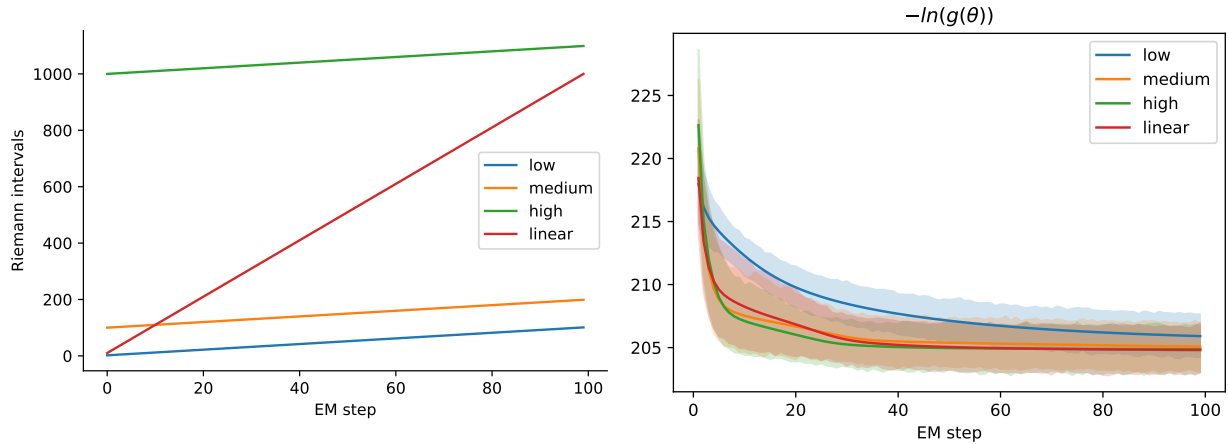


Fig. 2 (Right). Visual representation of the number of Riemann intervals over the EM steps for each profile φ_i . The total number of Riemann intervals computed over 100 EM iterations are: 5 150 for “low”, 14 950 for “medium”, 50 500 for “linear” and 104 950 for “high”. (Left). For each profile, average evolution of the negative log-likelihood, with standard deviation, over 50 simulations. The results are fairly similar, in particular between “medium”, “high” and “linear”.

with symmetric formulas for $\hat{\alpha}_2$, $\hat{\lambda}_2$ and $\hat{\sigma}_2$. For the simulations, we take $(\alpha_1, \alpha_2) = (1, 3)$, $(\lambda_1, \lambda_2) = (10, -10)$ and $(\sigma_1, \sigma_2) = (2, 3)$. From the previous experiment, we keep only the two least costly profiles: “low” $\varphi_1(n) := n + 1$ and “medium” $\varphi_2(n) := n + 100$. We also consider two new, sub-linear, profiles “square root” $\varphi_5(n) := \lfloor \sqrt{n} \rfloor + 1$ and “5 square root” $\varphi_6(n) := 5 \times \lfloor \sqrt{n} \rfloor$. $\varphi_5(n)$ and $\varphi_6(n)$ are designed to have linear complexity even in 2-dimensions.

The results of the EM algorithm runs are displayed on Fig. 3. On the left, we follow the number of Riemann squares mapping the 2D space. The difference in computational complexity between profiles is accentuated by the higher dimension. In particular, “medium” performs 6.7 times more computations than “low” and 18.4 times more than “5 square root”. However, on the right of Fig. 3, we observe that these three profiles perform similar optimisations. This observation justifies cutting

computation costs by using lower resolution profiles to compensate the higher dimension.

4 Tempered EM

4.1 Context and motivation

In this section, we consider another particular case of Deterministic Approximate EM: the Tempered EM (or “tmp-EM”). We first motivate this algorithm. Then, we prove that under mild conditions, it verifies the hypothesis of Theorem 1, hence has the state of the art EM convergence guarantees. In particular, we prove that the choice of the temperature profile is almost completely free.

When optimising a non-convex function, following the gradients leads to one of the local extrema closest to the initialisation. If the method was allowed to explore more the profile of the function to be optimised, it would encounter points with better values and areas with stronger gradients missed because of its early commitment to one of the nearest potential wells.

A very well known way to encourage such an exploratory behaviour is the tempering, also called annealing. In its simplest form, the function to optimised g is elevated to the power $\frac{1}{T_n}$: $g \mapsto g^{\frac{1}{T_n}}$. Where T_n is a temperature tending towards 1 as the number n of steps of the procedure increases. This manipulation equalises the value of the function in the different points of the space, renders the gradients less strong, and makes the potential wells less attractive the higher the temperature T_n is. As a result, the optimisation procedure is not incited to limit itself to its starting region. Additionally, the general shape of the function g , in particular the hierarchy of values, is still preserved, meaning that the early course of the algorithm is still made on a function replicating the reality. As T_n gets closer to 1, the optimised function becomes identical to g and the potential wells become attractive again. By this point, the assumption is that the algorithm will be in a better place than it was at the initialisation.

These concepts are put in application in many state of the art procedures. The most iconic maybe being the Simulated Annealing, introduced and developed in Kirkpatrick et al. (1983); Van Laarhoven and Aarts (1987); Aarts and Korst (1988), where in particular $T_n \rightarrow 0$ instead of 1. It is one of the few optimisation technique proven to find global optimum of non-convex functions. The Parallel Tempering (or Annealing MCMC) developed in Swendsen and Wang (1986); Geyer and Thompson (1995); Hukushima and Nemoto (1996) also makes use of these ideas to improve the MCMC simulation of a target probability distribution.

The idea of applying a tempering to a classical EM was introduced in the Deterministic Annealed EM of Ueda and Nakano (1998) with a specific decreasing temperature scheme. Another specific, non-monotonous, temperature scheme was later proposed by Naim and Gildea (2012). In both cases, theoretical convergence guarantees are lacking. In Allasonnière and Chevallier (2019), tempering is applied to the SAEM, and convergence guarantees for the resulting algorithm are provided with any temperature scheme $T_n \rightarrow 1$.

Here, we introduce the tmp-EM as a specific case of the Approximate EM of Section 2. We use the approximated distribution: $\tilde{p}_{n,\theta}(z) := p_{\theta}^{\frac{1}{T_n}}(z) / \int_{z'} p_{\theta}^{\frac{1}{T_n}}(z') dz' = h(z; \theta)^{\frac{1}{T_n}} / \int_{z'} h(z'; \theta)^{\frac{1}{T_n}} dz'$ (renormalised to sum to 1). Unlike Ueda and Nakano (1998) and Naim and Gildea (2012), we do not specify any temperature scheme T_n , and prove in the following Theorem 3 that, under very mild conditions on the model, any sequence $\{T_n\}_n \in (\mathbb{R}^*)^{\mathbb{N}}$, $T_n \xrightarrow[n \rightarrow \infty]{} 1$ guarantees the state of the art convergence.

Remark 2 Elevating $p_{\theta}(z)$ to the power $\frac{1}{T_n}$, as is done here and in Ueda and Nakano (1998); Naim and Gildea (2012), is not equivalent to elevating to the power $\frac{1}{T_n}$ the objective function $g(\theta)$, which would be expected for a typical annealed or tempered optimisation procedure. It is not equivalent either to elevating to the power $\frac{1}{T_n}$ the proxy function $\mathbb{E}_{z \sim p_{\theta_n}(z)} [h(z; \theta)]$ that is optimised in the M step. Instead, the weights $p_{\theta_n}(z)$ (or equivalently, the terms $h(z; \theta_n)$) used in the calculation of $\mathbb{E}_{z \sim p_{\theta_n}(z)} [h(z; \theta)]$ are the tempered terms. This still results in the desired behaviour and is only a more “structured” tempering. Indeed, with this tempering, it is the estimated distribution of the latent variable z that are made less unequivocal, with weaker modes, at each step. This forces the procedure to spend more time considering different configurations for those variables. Which renders as a result the optimised function $\mathbb{E}_{z \sim p_{\theta_n}(z)} [h(z; \theta)]$ more ambiguous regarding which θ is the best, just as intended. Then, when n large, the algorithm is allowed to converge, as $T_n \rightarrow 1$ and $\mathbb{E}_{z \sim \tilde{p}_{n,\theta}(z)} \rightarrow \mathbb{E}_{z \sim p_{\theta}(z)}$.

4.2 Theorem

We now give the convergence Theorem for the Approximate EM with the tempering approximation. In particular, this result highlights that there are almost no constraints on the temperature profile to achieve convergence.

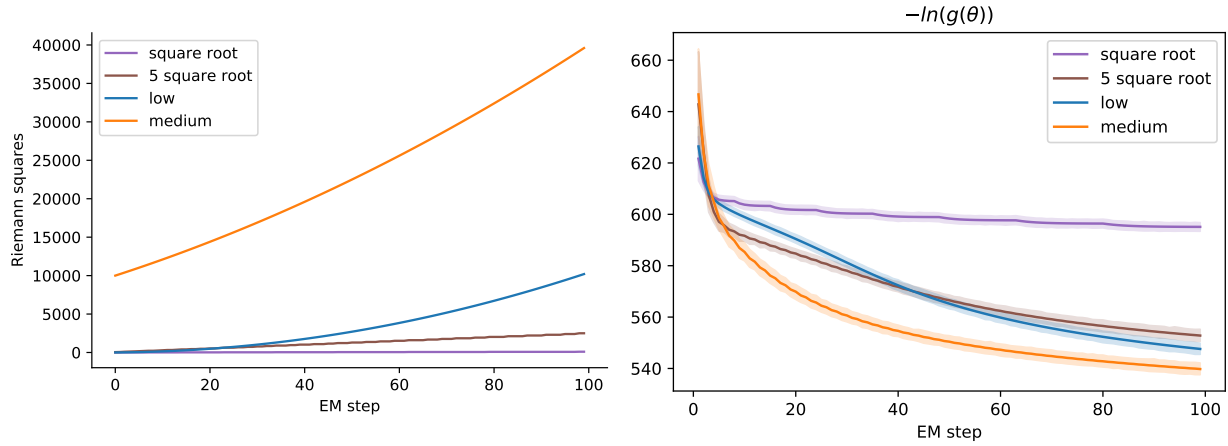


Fig. 3 (Right). Visual representation of the number of Riemann intervals over the EM steps for each profile φ_i . In higher dimension, the computational complexity of the profiles are very different. More precisely, the total number of Riemann squares computed over 100 EM iterations are: 4 534 for “square root”, 125 662 for “5 square root”, 348 550 for “low” and 2 318 350 for “medium”. (Left). For each profile, average evolution of the negative log-likelihood, with standard deviation, over 50 simulations. The “square root” profile performs poorly. However, the other three are comparable despite their different computational complexities.

Theorem 3 *Let T_n be a sequence of non-zero real numbers. Under conditions M1-3 of Theorem 1, the (Stable) Approximate EM with $\tilde{p}_{n,\theta}(z) := \frac{p_{\theta}^{\frac{1}{T_n}}(z)}{\int_z p_{\theta}^{\frac{1}{T_n}}(z') dz'}$, which we call “Tempered EM”, verifies all other remaining conditions of applicability of Theorem 1 as long as $T_n \xrightarrow{n \rightarrow \infty} 1$ and for any compact $K \in \Theta$, $\exists \epsilon \in]0, 1[$, $\forall \alpha \in \overline{B}(1, \epsilon)$:*

$$\begin{aligned} & - \sup_{\theta \in K} \int_z p_{\theta}^{\alpha}(z) dz < \infty \\ & - \forall u \in \llbracket 1, q \rrbracket, \sup_{\theta \in K} \int_z S_u^2(z) p_{\theta}^{\alpha}(z) dz < \infty \end{aligned}$$

Where $\overline{B}(1, \epsilon)$ is the closed ball centered in 1 and with radius ϵ in \mathbb{R} , and the index u of $S_u(z)$ indicates each of the real component of the $S(z) \in \mathcal{S} \subset \mathbb{R}^q$. The conditions on the integrability of $p_{\theta}^{\alpha}(z)$ and $S_u^2(z) p_{\theta}^{\alpha}(z)$ brought by the tempering are very mild. Indeed, in Section 4.4, we will show classical examples that easily verify the much stronger conditions: for any compact $K \in \Theta$, $\forall \alpha \in \mathbb{R}_+$,

$$\begin{aligned} & \sup_{\theta \in K} \int_z p_{\theta}^{\alpha}(z) dz < \infty, \\ & \forall u \in \llbracket 1, q \rrbracket, \sup_{\theta \in K} \int_z S_u^2(z) p_{\theta}^{\alpha}(z) dz < \infty. \end{aligned}$$

4.3 Sketch of proof

The detailed proof of Theorem 3 can be found in supplementary materials, we propose here a abbreviated version.

In order to apply Theorem 1, we need to verify five conditions. The three inevitable are M1, M2 and M3. The last two can either be that, \forall compact $K \in \Theta$:

$$\begin{cases} \int_z S_u^2(z) dz < \infty, \\ \sup_{\theta \in K} \int_z (\tilde{p}_{\theta,n}(z) - p_{\theta}(z))^2 dz \xrightarrow{n \rightarrow \infty} 0. \end{cases}$$

Or

$$\begin{cases} \sup_{\theta \in K} \int_z S_u^2(z) p_{\theta}(z) dz < \infty, \\ \sup_{\theta \in K} \int_z \left(\frac{\tilde{p}_{\theta,n}(z)}{p_{\theta}(z)} - 1 \right)^2 p_{\theta}(z) dz \xrightarrow{n \rightarrow \infty} 0. \end{cases}$$

The hypothesis of Theorem 3 already include M1, M2, M3 and:

$$\forall \text{ compact } K \in \Theta, \forall u, \sup_{\theta \in K} \int_z S_u^2(z) p_{\theta}(z) dz < \infty.$$

As a result, to apply Theorem 1, it is sufficient to verify that, with the tempering approximation, we have:

$$\sup_{\theta \in K} \int_z \left(\frac{\tilde{p}_{\theta,n}(z)}{p_{\theta}(z)} - 1 \right)^2 p_{\theta}(z) dz \xrightarrow{n \rightarrow \infty} 0.$$

The proof of Theorem 3 revolves around proving this result.

With a Taylor development in $\left(\frac{1}{T_n} - 1\right)$, which converges toward 0 when $n \rightarrow \infty$, we control the difference

$$\begin{aligned}
& (\tilde{p}_{\theta,n}(z) - p_{\theta}(z))^2: \\
& \left(\frac{p_{\theta}(z)^{\frac{1}{T_n}}}{\int_{z'} p_{\theta}(z')^{\frac{1}{T_n}}} - p_{\theta}(z) \right)^2 \\
& \leq 2 \left(\frac{1}{T_n} - 1 \right)^2 p_{\theta}(z)^2 \\
& \quad \times \left(\left(\ln p_{\theta}(z) e^{a(z,\theta,T_n)} \right)^2 A(\theta, T_n) + B(\theta, T_n) \right).
\end{aligned}$$

The terms $A(\theta, T_n)$, $B(\theta, T_n)$ and $a(z, \theta, T_n)$ come from the Taylor development. With the previous inequality, we control the integral of interest:

$$\begin{aligned}
& \int_z \frac{\left(\frac{p_{\theta}(z)^{\frac{1}{T_n}}}{\int_{z'} p_{\theta}(z')^{\frac{1}{T_n}}} - p_{\theta}(z) \right)^2}{p_{\theta}(z)} dz \\
& \leq 2 \left(\frac{1}{T_n} - 1 \right)^2 A(\theta, T_n) \int_z p_{\theta}(z) e^{2a(z,\theta,T_n)} \ln^2 p_{\theta}(z) dz \\
& \quad + 2 \left(\frac{1}{T_n} - 1 \right)^2 B(\theta, T_n).
\end{aligned} \tag{10}$$

$A(\theta, T_n)$ and $B(\theta, T_n)$ both have upper bounds involving $\int_z p_{\theta}(z)^{\frac{1}{T_n}} \ln p_{\theta}(z)$. In a similar fashion, the term $\int_z p_{\theta}(z) e^{2a(z,\theta,T_n)} \ln^2 p_{\theta}(z)$ is bounded by terms involving $\int_z p_{\theta}(z)^{\frac{2}{T_n}-1} \ln^2 p_{\theta}(z) dz$.

Thanks to the hypothesis of the Theorem, we prove that for any $\alpha \in \bar{B}(1, \epsilon)$ and $\theta \in K$ the two terms, $\int_z p_{\theta}(z)^{\alpha} \ln p_{\theta}(z)$ and $\int_z p_{\theta}(z)^{\alpha} \ln^2 p_{\theta}(z)$ are both upper bounded by a constant C independent of θ and α .

Since $T_n \xrightarrow{n \rightarrow \infty} 1$, then when n is large enough, $\frac{1}{T_n} \in \bar{B}(1, \epsilon)$ and $\frac{2}{T_n} - 1 \in \bar{B}(1, \epsilon)$ meaning that the previous result applies to the three terms $A(\theta, T_n)$, $B(\theta, T_n)$ and $\int_z p_{\theta}(z) e^{2a(z,\theta,T_n)} \ln^2 p_{\theta}(z) dz$: they are upper bounded by constants C_1 , C_2 and C_3 respectively, all independent of θ and T_n .

The inequality (10) then becomes:

$$\begin{aligned}
& \int_z \frac{1}{p_{\theta}(z)} \left(\frac{p_{\theta}(z)^{\frac{1}{T_n}}}{\int_{z'} p_{\theta}(z')^{\frac{1}{T_n}}} - p_{\theta}(z) \right)^2 dz \\
& \leq 2 \left(\frac{1}{T_n} - 1 \right)^2 C_1 C_2 + 2 \left(\frac{1}{T_n} - 1 \right)^2 C_3.
\end{aligned}$$

By taking the supremum in $\theta \in K$ and the limit when $n \rightarrow \infty$, we get the desired result:

$$\sup_{\theta \in K} \int_z \frac{1}{p_{\theta}(z)} \left(\frac{p_{\theta}(z)^{\frac{1}{T_n}}}{\int_{z'} p_{\theta}(z')^{\frac{1}{T_n}}} - p_{\theta}(z) \right)^2 dz \xrightarrow{n \rightarrow \infty} 0.$$

4.4 Examples of models that verify the conditions

In this section we illustrate that the conditions of Theorem 3 are easily met by common models. We take two examples, first the Gaussian Mixture Model (GMM) where the latent variables belong to a finite space, then the Poisson count with random effect, where the latent variables live in a continuous space.

In order to apply Theorem 3, we need to verify the conditions

- $M1$, $M2$ and $M3$
- for any compact $K \in \Theta$, $\exists \epsilon \in]0, 1[$, $\forall \alpha \in \bar{B}(1, \epsilon)$,

$$\sup_{\theta \in K} \int_z p_{\theta}^{\alpha}(z) dz < \infty,$$

$$\forall u, \sup_{\theta \in K} \int_z S_u^2(z) p_{\theta}^{\alpha}(z) dz < \infty.$$

As previously stated, in both examples, we will actually verify the much stronger conditions: for any compact $K \in \Theta$, $\forall \alpha \in \mathbb{R}_+^*$:

$$\begin{cases} \sup_{\theta \in K} \int_z p_{\theta}^{\alpha}(z) dz < \infty, \\ \forall u, \sup_{\theta \in K} \int_z S_u^2(z) p_{\theta}^{\alpha}(z) dz < \infty. \end{cases}$$

4.4.1 Gaussian Mixture Model

Despite being one of the most common models the EM is applied to, the GMM have many known irregularities and pathological behaviours, see [Titterton et al. \(1985\)](#); [Ho et al. \(2016\)](#). Although some recent works, such as [Dwivedi et al. \(2018, 2020\)](#), tackled the theoretical analysis of EM for GMM, none of the convergence results for the traditional EM and its variants proposed by [Wu \(1983\)](#); [Lange \(1995\)](#); [Delyon et al. \(1999\)](#); [Fort and Moulines \(2003\)](#) apply to the GMM. The hypothesis that the GMM fail to verify is the condition that the level lines have to be compact ($M2(d)$ in this paper). All is not lost however for the GMM, indeed, the model verifies all the other hypothesis of the general Theorem 1 as well as the tempering hypothesis of Theorem 3. Moreover, in this paper as in the others, the only function of the unverified hypothesis $M2(d)$ is to ensure in the proof that the EM sequence stays within a compact. The latter condition is the actual relevant property to guarantee convergence at this stage of the proof. This means that, in practice, if an tempered EM sequence applied to a GMM is observed to remain within a compact, then all the conditions for convergence are met, Theorem 3 applies, and the sequence is guaranteed to converge towards a critical point of the likelihood function.

In the following, we give more details on the GMM likelihoods and the theorem hypotheses they verify. First,

note that the GMM belongs to the curved exponential family with the complete likelihood:

$$h(z; \theta) = \prod_{i=1}^N \sum_{k=1}^K \exp \left(\frac{1}{2} \left(- (x^{(i)} - \mu_k)^T \Theta_k (x^{(i)} - \mu_k) + \ln(|\Theta_k|) + 2 \ln(\pi_k) - p \ln(2\pi) \right) \right) \mathbb{1}_{z^{(i)}=k}, \quad (11)$$

and the observed likelihood:

$$g(\theta) = \prod_{i=1}^N \sum_{k=1}^K \exp \left(\frac{1}{2} \left(- (x^{(i)} - \mu_k)^T \Theta_k (x^{(i)} - \mu_k) + \ln(|\Theta_k|) + 2 \ln(\pi_k) - p \ln(2\pi) \right) \right). \quad (12)$$

This is an exponential model with parameter:

$$\theta := \left(\{\pi_k\}_{k=1}^K, \{\mu_k\}_{k=1}^K, \{\Theta_k\}_{k=1}^K \right) \in \left\{ \{\pi_k\}_k \in [0, 1]^K \mid \sum_k \pi_k = 1 \right\} \otimes \mathbb{R}^{p \times K} \otimes S_p^{++K}.$$

The verification of conditions $M1-3$ for the GMM (expt $M2(d)$ of course) is a classical exercise since these are the conditions our Theorem shares with any other EM convergence result on the exponential family. We focus here on the hypothesis specific to our Deterministic Approximate EM.

Condition on $\int_z p_\theta^\alpha(z) dz$ Let $\alpha \in \mathbb{R}_+^*$, in the finite mixture case, the integrals on z are finite sums:

$$\int_z p_\theta^\alpha(z) dz = \sum_k p_\theta^\alpha(z = k).$$

Which is continuous in θ since $\theta \mapsto p_\theta(z = k) = h(z = k; \theta)/g(\theta)$ is continuous. Hence

$$\forall \alpha \in \mathbb{R}_+^*, \quad \sup_{\theta \in K} \int_z p_\theta^\alpha(z) dz < \infty.$$

Condition on $\int_z S_u^2(z) p_\theta^\alpha(z) dz$ The previous continuity argument is still valid.

4.4.2 Poisson count with random effect

This model is discussed in [Fort and Moulines \(2003\)](#), the authors prove, among other things, that this model verifies the conditions $M1-3$.

The complete likelihood of the model, not accounting for irrelevant constants, is:

$$h(z; \theta) = e^{\theta \sum_k Y_k} \exp \left(-e^\theta \sum_k e^{z_k} \right). \quad (13)$$

$g(\theta) = \int_z h(z; \theta) dz$ can be computed analytically up to a constant:

$$\begin{aligned} g(\theta) &= \int_{z \in \mathbb{R}^d} h(z; \theta) dz \\ &= e^{\theta \sum_k Y_k} \int_{z \in \mathbb{R}^d} \exp \left(-e^\theta \sum_k e^{z_k} \right) dz \\ &= e^{\theta \sum_k Y_k} \prod_{k=1}^d \int_{z_k \in \mathbb{R}} \exp(-e^\theta e^{z_k}) dz_k \\ &= e^{\theta \sum_k Y_k} \left(\int_{u \in \mathbb{R}_+} \frac{\exp(-u)}{u} du \right)^d \\ &= e^{\theta \sum_k Y_k} E_1(0)^d, \end{aligned} \quad (14)$$

where $E_1(0)$ is a finite, non zero, constant, called “exponential integral”, in particular independent of α and θ .

Condition on $\int_z p_\theta^\alpha(z) dz$ Let K be a compact in Θ . We have $p_\theta(z) = \frac{h(z; \theta)}{g(\theta)}$. Let us compute $\int_z h(z; \theta)^\alpha$ for any positive α . The calculations work as in Eq. (14):

$$\begin{aligned} \int_{z \in \mathbb{R}^d} h(z; \theta)^\alpha &= e^{\alpha \theta \sum_k Y_k} \prod_{k=1}^d \int_{z_k \in \mathbb{R}} \exp(-\alpha e^\theta e^{z_k}) dz_k \\ &= e^{\alpha \theta \sum_k Y_k} E_1(0)^d. \end{aligned}$$

Hence:

$$\int_z p_\theta^\alpha(z) dz = E_1(0)^{(1-\alpha)d}.$$

Since $E_1(0)$ is finite, non zero, and independent of θ , we easily have:

$$\forall \alpha \in \mathbb{R}_+^*, \quad \sup_{\theta \in K} \int_z p_\theta^\alpha(z) dz < \infty.$$

θ does not even have to be restricted to a compact.

Condition on $\int_z S_u^2(z) p_\theta^\alpha(z) dz$ Let K be a compact in Θ and α a positive real number.

In this Poisson count model, $S(z) = \sum_k e^{z_k} \in \mathbb{R}$. We have:

$$S^2(z) p_\theta^\alpha(z) = \left(\sum_k e^{z_k} \right)^2 \frac{\exp(-\alpha e^\theta \sum_k e^{z_k})}{E_1(0)^{\alpha d}}. \quad (15)$$

First, let us prove that the integral is finite for any θ . We introduce the variables $u_k := \sum_{l=1}^k e^{z_l}$. The Jacobi matrix is triangular and its determinant is $\prod_k e^{z_k} = \prod_k u_k$.

$$\int_z S^2(z) p_\theta^\alpha(z) dz = \frac{\int_{z \in \mathbb{R}^d} (\sum_k e^{z_k})^2 \exp(-\alpha e^\theta \sum_k e^{z_k}) dz}{E_1(0)^{\alpha d}}.$$

Which is proportional to:

$$\int_{u_1=0}^{+\infty} u_1 \int_{u_2=u_1}^{+\infty} u_2 \dots \int_{u_d=u_{d-1}}^{+\infty} u_d^3 e^{-\alpha e^\theta u_d} du_d \dots du_2 du_1.$$

Where we removed the finite constant $\frac{1}{E_1(0)^{\alpha d}}$ for clarity. This integral is finite for any θ because the exponential is the dominant term around $+\infty$. Let us now prove that $\theta \mapsto \int_z S^2(z) p_\theta^\alpha(z) dz$ is continuous. From Eq. (15), we have that

- $z \mapsto S^2(z) p_\theta^\alpha(z)$ is measurable on \mathbb{R}^d .
- $\theta \mapsto S^2(z) p_\theta^\alpha(z)$ is continuous on K (and on $\Theta = \mathbb{R}$).
- With $\theta_M := \min_{\theta \in K} \theta$, then $\forall \theta \in K$, $0 \leq S^2(z) p_\theta^\alpha(z) \leq S^2(z) p_{\theta_M}^\alpha(z)$

Since we have proven that $S^2(z) p_{\theta_M}^\alpha(z) < \infty$, then we can apply the interversion Theorem and state that $\theta \mapsto \int_z S^2(z) p_\theta^\alpha(z) dz$ is continuous.

It directly follows that:

$$\forall \alpha \in \mathbb{R}_+^*, \quad \sup_{\theta \in K} \int_z S^2(z) p_\theta^\alpha(z) dz < \infty.$$

Note that after the change of variable, the integral could be computed explicitly, but involves d successive integration of polynomial \times exponential function products of the form $P(x)e^{-\alpha e^\theta x}$. This would get tedious, especially since after each successful integration, the product with the next integration variable u_{k-1} increases by one the degree of the polynomial, i.e. starting from 3, the degree ends up being $d+2$. We chose a faster path.

4.5 Experiments with Mixtures of Gaussian

4.5.1 Context and experimental protocol

In this section, we will assess the capacity of tmp-EM to escape from deceptive local maxima, on a very well

known toy example: likelihood maximisation within the Gaussian Mixture Model. We confront the algorithm to situations where the true classes have increasingly more ambiguous positions, combined with initialisations designed to be hard to escape from. Although the EM is an optimisation procedure, and the log-likelihood reached is a critical metric, in this example, we put more emphasis on the correct positioning of the cluster centroids, that is to say on the recovery of the μ_k . The other usual metrics are also in favour of tmp-EM, and can be found in supplementary materials.

For the sake of comparison, the experimental design is similar to the one in Allasonnière and Chevallier (2019) on the tmp-SAEM. It is as follows: we have three clusters of similar shape and same weight. One is isolated and easily identifiable. The other two are next to one another, in a more ambiguous configuration. Fig. 4 represents the three, gradually more ambiguous configurations. Each configuration is called a “parameter family”. We use two different initialisation types to reveal the behaviours of the two EMs. The first - which we call “*barycenter*” - puts all three initial centroids at the centre of mass of all the observed data points. However, none of the EM procedures would move from this initial state if the three GMM centroids were at the exact same position, hence we actually apply a tiny perturbation to make them all slightly distinct. The blue crosses on Fig. 5 represent a typical *barycenter* initialisation. With this initialisation method, we assess whether the EM procedures are able to correctly estimate the positions of the three clusters, despite the ambiguity, when starting from a fairly neutral position, providing neither direction nor misdirection. On the other hand, the second initialisation type - which we call “*2v1*” - is voluntarily misleading the algorithm by positioning two centroids on the isolated right cluster and only one centroid on the side of the two ambiguous left clusters. The blue crosses on Fig. 6 represent a typical *2v1* initialisation. This initialisation is intended to assess whether the methods are able to escape the potential well in which they start and make their centroids traverse the empty space between the left and right clusters to reach their rightful position. For each of the three parameter families represented on Fig. 4, 1000 datasets with 500 observations each are simulated, and the two EMs are ran with both the *barycenter* and the *2v1* initialisation. Regarding the temperature profile of tmp-EM, the only constraint is that $T_n \rightarrow 1$. We use an oscillating profile inspired from Allasonnière and Chevallier (2019): $T_n = th(\frac{n}{2r}) + (T_0 - b\frac{2\sqrt{2}}{3\pi})a^{n/r} + b \text{sinc}(\frac{3\pi}{4} + \frac{n}{r})$. Where $0 < T_0$, $0 < r$, $0 < b$ and $0 < a < 1$. The oscillations in this profile are meant to achieve a two-regimes behaviour. When the temperature reaches low values, the

convergence speed is momentarily increased which has the effect of “lockin-in” some of the most obviously good decisions of the algorithm. Then, the temperature is re-increased to continue the exploration on the other, more ambiguous, parameters. Those two regimes are alternated in succession with gradually smaller oscillations, resulting in a multi-scale procedure that “locks-in” gradually harder decisions. For some hyper-parameter combinations, the sequence T_n can have a (usually small) finite number of negative values. Since only the asymptotic behaviour of T_n is the step n matters for convergence, then the theory allows a finite number of negative values. However, in practice, at least for the sake of interpretation, one may prefer to use only positive values for T_n . In which case, one can either restrain themselves to parameter combinations that result in no negatives values for T_n , or enforce positivity by taking $T_n \leftarrow \max(T_n, \epsilon)$ with a certain $\epsilon > 0$.

For our experiments, we select the hyper-parameter values with a grid-search. The “normalised” *sinc* function is used $\text{sinc}(x) = \sin(\pi x)/(\pi x)$ and the chosen tempering parameters are $T_0 = 5$, $r = 2$, $a = 0.6$, $b = 20$ for the experiments with the *barycenter* initialisation, and $T_0 = 100$, $r = 1.5$, $a = 0.02$, $b = 20$ for the *2v1* initialisation. Although, we observe that in the case of *2v1*, the oscillations are not critical, and a simple decreasing exponential profile: $T_n = 1 + (T_0 - 1) \exp(-r \cdot n)$, with $T_0 = 100$ and $r = 1.5$, works as well. We have two different sets of tempering hyper-parameters values, one for each of the two very different initialisation types. However, these values then remain the same for the three different parameter families and for every data generation within them. This underlines that the method is not excessively sensitive to the tempering parameters, and that the prior search for good hyper-parameter values is a worthwhile time investment. Likewise, a simple experiment with 6 clusters, in supplementary materials, demonstrates that the same hyper-parameters can be kept over different initialisation (and different data generations as well) when they were made in a non-adversarial way, by drawing random initial centroids uniformly among the data points.

4.5.2 Quantitative analysis

In this section, we quantify the performances of EM and tmp-EM over all the simulations.

Fig. 5 and 6 depict the results of one typical simulation for each of the three ambiguity level (the three parameter families) starting from the *barycenter* and *2v1* initialisation respectively. The simulated data is represented by the green crosses. The initial centroids are in blue. The orange cross represents the estimated cen-

troids positions $\hat{\mu}_k$, and the orange confidence ellipses are visual representations of the estimated covariance matrices $\hat{\Sigma}_k$. In supplementary materials, we show step by step the path taken by the estimated parameters of tmp-EM before convergence, providing much more detail on the method’s behaviours.

On these examples, we note that tmp-EM is more correct than EM. The results over all simulations are aggregated in Table 1, and confirm this observation.

Table 1 presents the average and the standard deviation of the relative l_2 error on μ_k of the EMs. For each category, the better result over EM and tmp-EM is highlighted in bold. The recovery of the true class averages μ_k is spotlighted as it is the essential success metric for this experiment.

First we focus on the effect of the different initialisations and placement of (μ_1, μ_2) on the performance of the classical EM. In the first parameter family of Table 1, μ_1 and μ_2 are still far from one another. The relative error on these two positions is around 0.50 when the initialisation is a the neutral position at the barycenter of the dataset, and 1.50 when the initialisation is made by placing two centroids in the right cluster (*2v1*), which is a much more adversarial initialisation. In the second parameter family, μ_1 and μ_2 are getting closer. The relative error with the *barycenter* initialisation has doubled to reach 1.00, and, with the adversarial *2v1*, it has increased to 1.70. Finally, in the third parameter family, where μ_1 and μ_2 are so close that their distributions are hard to distinguish with the naked eye, the relative error with the *barycenter* initialisation has gained another 0.50 points to reach over 1.50, which was the initial error level with the *2v1* initialisation when μ_1 and μ_2 were well separated (parameter family 1). In this very ambiguous setting however, the relative error with *2v1* initialisation has gone up to around 1.80-1.90. As expected, we see that the performances are always hindered in average by the *2v1* initialisation, and that they also worsen when the relative positions of μ_1 and μ_2 become more ambiguous, regardless of the initialisation. The *barycenter* initialisation however is the one that suffers the most from the increasing ambiguity, gaining 0.5 points of relative error at every transition, whereas *2v1* gain “only” around 0.2 points.

We compare these results and their progression with the ones of tmp-EM in Table 1. In the first parameter family - the least ambiguous situation - the relative errors on μ_1 and μ_2 are around 0.05 with the *barycenter* initialisation and 0.30 with *2v1*. In other words, with the tempered E step, we divide by 10 and 5 respectively the relative errors with the *barycenter* and *2v1* initialisation. In the next position of μ_1 and μ_2 , in the second parameter family, the relative error with the

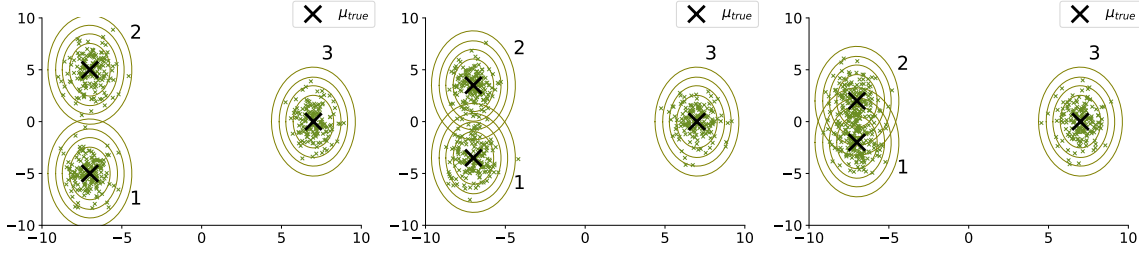


Fig. 4 500 sample points from a Mixture of Gaussians with 3 classes. The true centroid of each Gaussian are depicted by black crosses, and their true covariance matrices are represented by the confidence ellipses of level 0.8, 0.99 and 0.999 around the centre. There are three different versions of the true parameters. From left to right: the true μ_k of the two left clusters (μ_1 and μ_2) are getting closer while everything else stays identical.

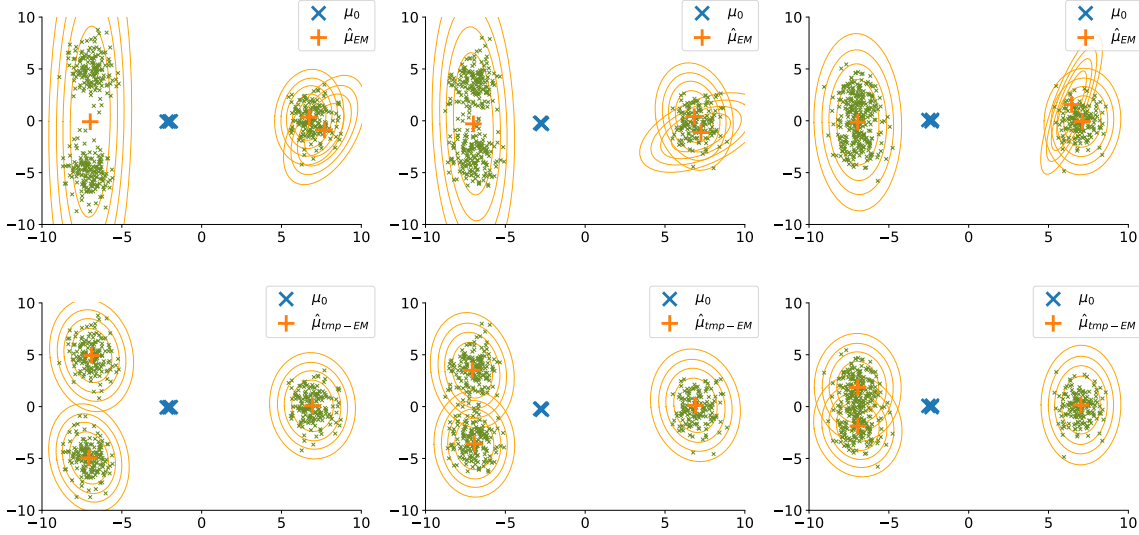


Fig. 5 Typical final positioning of the centroids by EM (first row) and tmp-EM (second row) **when the initialisation is made at the barycenter of all data points** (blue crosses). The three columns represent the three gradually more ambiguous parameter sets. Each figure represents the positions of the estimated centroids after convergence of the EM algorithms (orange cross), with their estimated covariance matrices (orange confidence ellipses). In each simulation, 500 sample points were drawn from the real GMM (small green crosses). In those example, tmp-EM managed to correctly identify the position of the three real centroids.

barycenter initialisation is now around 0.10, staying 10 times smaller than without tempering. With *2v1*, the relative error stayed fairly stable, reaching now 0.35 in average, and remaining approximately 5 times smaller than without tempering. We underline that up until this point (parameter families 1 and 2), the standard deviation of these errors was 3 times smaller with tempering in the case of the *barycenter* initialisation, and around 2 times smaller in the case of the *2v1* initialisation. In the final configuration, parameter family 3, the relative errors with tempering are 0.30 with the *barycenter* initialisation (5 times smaller than without tempering) and 0.40 with the *2v1* initialisation (more than 4.5 times smaller than without tempering). More-

over, the standards deviations are at least 1.8 times smaller with tempering. We note that, in similar fashion to EM, the errors on μ_1 and μ_2 with the *barycenter* initialisation reached, in the most ambiguous configuration, the level of error seen with the *2v1* initialisation in the least ambiguous situation: 0.30. Which, as stated, remains 5 times smaller than the corresponding level of error without tempering: 1.50.

In the end, the progression of errors when μ_1 and μ_2 get closer is alike between EM and tmp-EM: the *barycenter* initialisation is the most affected, the *2v1* initialisation error being higher but fairly stable. However the level of error is much smaller with tmp-EM, being 5 to 10 times smaller in the case of the *barycenter* initialisation, and

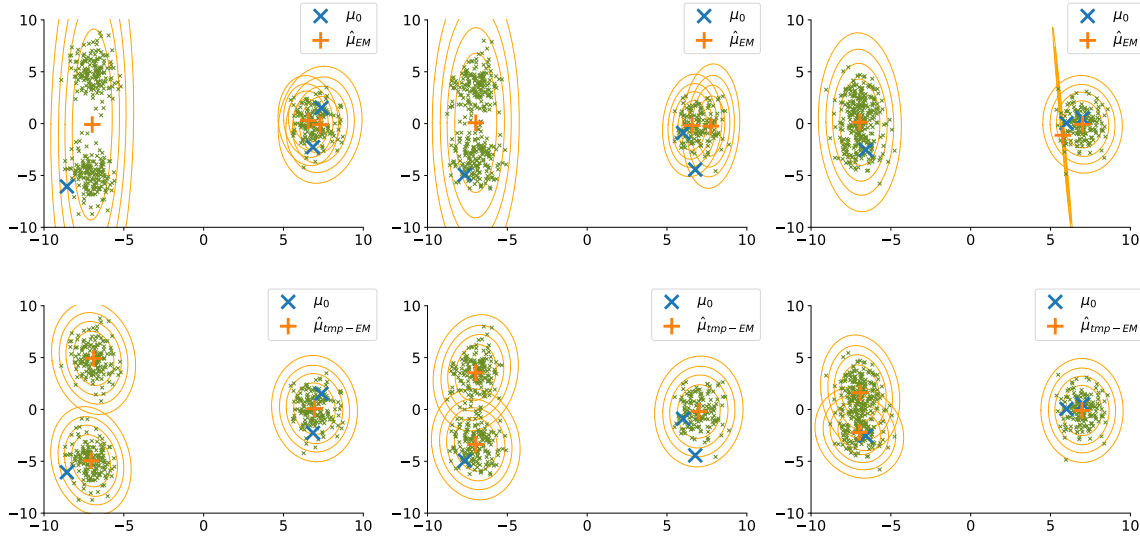


Fig. 6 Typical final positioning of the centroids by EM (first row) and tmp-EM (second row) **when the initialisation is made by selecting two points in the isolated cluster and one in the lower ambiguous cluster** (blue crosses). The three columns represent the three gradually more ambiguous parameter sets. Each figure represents the positions of the estimated centroids after convergence of the EM algorithms (orange cross), with their estimated covariance matrices (orange confidence ellipses). In each simulation, 500 sample points were drawn from the real GMM (small green crosses). In those examples, although EM kept two centroids on the isolated cluster, tmp-EM managed to correctly identify the position of the three real centroids.

4.5 to 5 times smaller for the *2v1* initialisation. Similarly, the standard deviation around those average levels is 1.8 to 2 times smaller with tmp-EM.

These quantitative results on the reconstruction error of μ_1 and μ_2 confirm exactly what was observed on the illustrative examples: with tempering, the EM procedure is much more likely to discern the true position of the three clusters regardless of the initialisation, and able to reach a very low error rate even with the most adversarial initialisations. To bolster this last point, we underline that even in the worst case scenario, *2v1* initialisation and very close μ_1 and μ_2 , tmp-EM still outperforms EM in the best scenario, *barycenter* initialisation and well separated clusters, with an error rate of 0.40 versus 0.50.

5 Tempered Riemann approximation EM

5.1 Context, Theorem and proof

The Riemann approximation of Section 3 makes the EM computations possible in hard cases, when the conditional distribution has no analytical form for instance. It is an alternative to the many stochastic approximation methods (SAEM, MCMC-SAEM...) that are commonly used in those cases. The tempering approximation of Section 4 is used to escape the initialisation by allowing the procedure to explore more the likelihood

profile before committing to convergence. We showed that both these approximation are particular cases of the wider class of Deterministic Approximate EM, introduced in Section 2. However, since they fulfil different purposes, it is natural to use them in coordination and not as alternatives of one another. In this section, we introduce another instance of the Approximate EM: a combination of the tempered and Riemann sum approximations. This “tempered Riemann approximation EM” (tmp-Riemann approximation) can compute EM steps when there is no closed form thanks to the Riemann sums as well as escape the initialisation thanks to the tempering. For a bounded latent variable $z \in [0, 1]$, we define the approximation as: $\tilde{p}_{n,\theta}(z) := h(\lfloor nz \rfloor / n; \theta)^{\frac{1}{T_n}} / \int_{\mathcal{Z}} h(\lfloor nz' \rfloor / n; \theta)^{\frac{1}{T_n}} dz'$, for a sequence $\{T_n\}_n \in (\mathbb{R}_+^*)^{\mathbb{N}}$, $T_n \xrightarrow{n \rightarrow \infty} 1$.

In the following Theorem, we prove that the tempered Riemann approximation EM verifies the applicability conditions of Theorem 1 with no additional hypothesis from the regular Riemann approximation EM covered by Theorem 2.

Theorem 4 *Under conditions M1 – 3 of Theorem 1, and when z is bounded, the (Stable) Approximate EM with $\tilde{p}_{n,\theta}(z) := \frac{h(\lfloor nz \rfloor / n; \theta)^{\frac{1}{T_n}}}{\int_{\mathcal{Z}} h(\lfloor nz' \rfloor / n; \theta)^{\frac{1}{T_n}} dz'}$, which we call “tempered Riemann approximation EM”, verifies the remain-*

Table 1 Average and standard deviation of the relative error on μ_k , $\frac{\|\hat{\mu}_k - \mu_k\|^2}{\|\mu_k\|^2}$, made by EM and tmp-EM over 1000 simulated dataset with two different initialisations. The three different parameter families, described in Fig. 4, correspond to increasingly ambiguous positions of classes 1 and 2. For both initialisations type, the identification of these two clusters is drastically improved by the tempering.

		EM		tmp-EM	
Parameter family	cl.	barycenter	2v1	barycenter	2v1
1	1	0.52 (1.01)	1.52 (1.24)	0.04 (0.26)	0.29 (0.64)
	2	0.55 (1.05)	1.53 (1.25)	0.05 (0.31)	0.30 (0.64)
	3	0.01 (0.06)	0.01 (0.03)	0.03 (0.17)	0.03 (0.19)
2	1	1.00 (1.42)	1.69 (1.51)	0.09 (0.47)	0.37 (0.86)
	2	1.03 (1.44)	1.71 (1.52)	0.12 (0.57)	0.32 (0.79)
	3	0.01 (0.05)	0.02 (0.03)	5.10⁻³ (0.05)	0.04 (0.22)
3	1	1.56 (1.75)	1.79 (1.77)	0.31 (0.97)	0.39 (0.98)
	2	1.51 (1.74)	1.88 (1.76)	0.30 (0.93)	0.39 (0.97)
	3	0.02 (0.04)	0.02 (0.04)	0.01 (0.04)	0.07 (0.30)

ing conditions of applicability of Theorem 1 as long as $z \mapsto S(z)$ is continuous and $\{T_n\}_n \in (\mathbb{R}_+^*)^{\mathbb{N}}$, $T_n \xrightarrow{n \rightarrow \infty} 1$.

Proof This proof of Theorem 4 is very similar to the proof of Theorem 2 for the regular Riemann approximation EM. The first common element is that for the tempered Riemann approximation EM, the only remaining applicability condition of the general Theorem 1 to prove is also:

$$\forall \text{compact } K \subseteq \Theta, \sup_{\theta \in K} \int_z (\tilde{p}_{\theta,n}(z) - p_{\theta}(z))^2 dz \xrightarrow{n \rightarrow \infty} 0.$$

In the proof of Theorem 2, we proved that having the uniform convergence of the approximated complete likelihood $\{\tilde{h}_n\}_n$ towards the real h - with both $\tilde{h}_n(z; \theta)$ and $h(z; \theta)$ uniformly bounded - was sufficient to fulfil this condition. Hence, we prove in this section that these sufficient properties still hold, even with the tempered Riemann approximation, where $\tilde{h}_n(z; \theta) := h(\lfloor nz \rfloor / n; \theta)^{\frac{1}{T_n}}$. We recall that $h(z; \theta)$ hence uniformly continuous on the compact set $[0, 1] \times K$, and verifies:

$$0 < m \leq h(z; \theta) \leq M < \infty.$$

Where m and M are constants independent of z and θ . Since $T_n > 0$, $T_n \xrightarrow{n \rightarrow \infty} 1$, then the sequence $\{1/T_n\}_n$ is bounded. Since $\tilde{h}_n(z; \theta) = h(\lfloor nz \rfloor / n; \theta)^{\frac{1}{T_n}}$, with $0 < m \leq h(\lfloor nz \rfloor / n; \theta) \leq M < \infty$ for any z, θ and n , then we also have:

$$0 < m' \leq \tilde{h}_n(z; \theta) \leq M' < \infty,$$

with m' and M' constants independent of z, θ and n . We have seen in the proof of Theorem 2, that:

$$\forall \epsilon > 0, \exists N \in \mathbb{N}, \forall n \geq N, \forall (z, \theta) \in [0, 1] \times K, \\ |h(z; \theta) - h(\lfloor nz \rfloor / n; \theta)| \leq \epsilon.$$

To complete the proof, we control in a similar way the difference $h(\lfloor nz \rfloor / n; \theta) - h(\lfloor nz \rfloor / n; \theta)^{\frac{1}{T_n}}$. The function $(h, T) \in [m, M] \times [T_{min}, T_{max}] \mapsto h^{\frac{1}{T}} \in \mathbb{R}$ is continuous on a compact, hence uniformly continuous in (h, T) . As a consequence: $\forall \epsilon > 0, \exists \delta > 0, \forall (h, h') \in [m, M]^2, (T, T') \in [T_{min}, T_{max}]^2$,

$$|h - h'| \leq \delta \text{ and } |T - T'| \leq \delta \implies \left| h^{\frac{1}{T}} - (h')^{\frac{1}{T'}} \right| \leq \epsilon.$$

Hence, with $N \in \mathbb{N}$ such that $\forall n \geq N, |T_n - 1| \leq \delta$, we have:

$$\forall n \geq N, \forall (z, \theta) \in [0, 1] \times K, \\ \left| h(\lfloor nz \rfloor / n; \theta) - h(\lfloor nz \rfloor / n; \theta)^{\frac{1}{T_n}} \right| \leq \epsilon.$$

In the end, $\forall \epsilon > 0, \exists N \in \mathbb{N}, \forall n \geq N, \forall (z, \theta) \in [0, 1] \times K$:

$$\begin{aligned} \left| h(z; \theta) - \tilde{h}_n(z; \theta) \right| &= \left| h(z; \theta) - h(\lfloor nz \rfloor / n; \theta)^{\frac{1}{T_n}} \right| \\ &\leq |h(z; \theta) - h(\lfloor nz \rfloor / n; \theta)| \\ &\quad + \left| h(\lfloor nz \rfloor / n; \theta) - h(\lfloor nz \rfloor / n; \theta)^{\frac{1}{T_n}} \right| \\ &\leq 2\epsilon. \end{aligned}$$

In other words, we have the uniform convergence of $\{\tilde{h}_n\}$ towards h . From there, we conclude following the same steps as in the proof of Theorem 2.

5.2 Application to a Gaussian model with the Beta prior

We illustrate the method with the model of Section 3.3:

$$h(z; \theta) = \frac{\alpha z^{\alpha-1}}{\sqrt{2\pi\sigma^2}} \exp\left(-\frac{(y - \lambda z)^2}{2\sigma^2}\right).$$

We apply the tempered Riemann approximation. As in Section 3.3, the resulting conditional probability density is a step function defined by the n different values it takes on $[0, 1]$. For the observation $x^{(i)}$, $\forall k \in \llbracket 0, n-1 \rrbracket$:

$$\tilde{p}_{\theta,n}^{(i)}\left(\frac{k}{n}\right) = \frac{h^{(i)}\left(\frac{k}{n}; \theta\right)^{\frac{1}{T_n}}}{\frac{1}{n} \sum_{l=0}^{n-1} h^{(i)}\left(\frac{l}{n}; \theta\right)^{\frac{1}{T_n}}}.$$

The M step, seen in Eq. (9), is unchanged. We compare the tempered Riemann EM to the simple Riemann EM on a case where the parameters are ambiguous. With real parameters $\alpha = 0.1, \lambda = 10, \sigma = 0.8$, for each of the 100 simulations, the algorithms are initialised at $\alpha_0 = 10, \lambda_0 = 1, \sigma_0 = 7$. The initialisation is somewhat adversarial, since the mean and variance of the marginal distribution of y are approximately the same with the real of the initialisation parameter, even though the distribution is different. Fig. 7 shows that the tempered Riemann EM better escapes the initialisation than the regular Riemann EM, and reaches errors on the parameters orders of magnitude below. The tempering parameters are here $T_0 = 150, r = 3, a = 0.02, b = 40$.

6 Conclusions

We proposed the Deterministic Approximate EM class to bring together the many possible deterministic approximations of the E step. We proved a unified Theorem, with mild conditions on the approximation, which ensures the convergence of the algorithms in this class. Then, we showcased members of this class that solve the usual practical issues of the EM algorithm. For intractable E step, we introduced the Riemann approximation EM, a less parametric and deterministic alternative to the extensive family of MC-EM. We showed on an empirical intractable example how the Riemann approximation EM was able to increase the likelihood and recover every parameter in a satisfactory manner with its simplest design, and no hyper parameter optimisation.

For cases where one wants to improve the solution of the EM, we proved that the tempered EM, introduced under a different form in Ueda and Nakano (1998), is a specific case of the Deterministic Approximate EM. Moreover, we showed that the commonly used models benefit from the convergence property as long as the

temperature profile converges towards 1. This justifies the use of many more temperature profiles than the ones tried in Ueda and Nakano (1998) and Naim and Gildea (2012). We ran an in-depth empirical comparison between tmp-EM and the regular EM. In particular, we showed how tmp-EM was able to escape from adversarial initial positions, a task that sometimes required complex non-monotonous temperature schemes, which are covered by our Theorem.

Finally, we added the Riemann approximation in order to apply the tempering in intractable cases. We were then able to show that the tmp-Riemann approximation massively improved the performances of the Riemann approximation, when the initialisation is ambiguous.

Future works will improve both methods. The Riemann approximation will be generalised to be applicable even when the latent variable is not bounded, and an intelligent slicing of the integration space will improve the computational performances in high dimension. Regarding the tempered EM, since the theory allows the usage of any temperature profile, the natural next step is to look for efficient profiles with few hyper-parameters for fast tuning. Afterwards, implementing an adaptive tuning of the temperature parameters during the procedure will remove the necessity for preliminary grid search altogether.

Acknowledgments

The research leading to these results has received funding from the European Research Council (ERC) under grant agreement No 678304, European Union's Horizon 2020 research and innovation program under grant agreement No 666992 (EuroPOND) and No 826421 (TVB-Cloud), and the French government under management of Agence Nationale de la Recherche as part of the "Investissements d'avenir" program, reference ANR-19-P3IA-0001 (PRAIRIE 3IA Institute) and reference ANR-10-IAIHU-06 (IHU-A-ICM).

References

- Aarts E, Korst J (1988) Simulated annealing and Boltzmann machines. New York, NY; John Wiley and Sons Inc.
- Allasonnière S, Chevallier J (2019) A New Class of EM Algorithms. Escaping Local Minima and Handling Intractable Sampling, URL <https://hal.archives-ouvertes.fr/hal-02044722>, working paper or preprint
- Allasonnière S, Kuhn E, Trouvé A, et al. (2010) Construction of bayesian deformable models via a

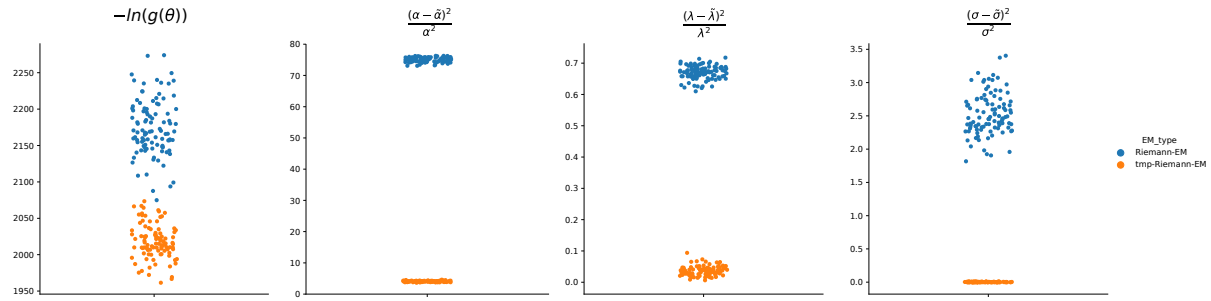


Fig. 7 Results over many simulations of the Riemann EM and tmp-Riemann EM on the Beta-Gaussian model. The tempered Riemann EM reaches relative errors on the real parameters that are orders of magnitude below the Riemann EM with no temperature. The likelihood reached is also lower with the tempering.

- stochastic approximation algorithm: a convergence study. *Bernoulli* 16(3):641–678
- Balakrishnan S, Wainwright MJ, Yu B, et al. (2017) Statistical guarantees for the em algorithm: From population to sample-based analysis. *The Annals of Statistics* 45(1):77–120
- Booth JG, Hobert JP (1999) Maximizing generalized linear mixed model likelihoods with an automated monte carlo em algorithm. *Journal of the Royal Statistical Society: Series B (Statistical Methodology)* 61(1):265–285
- Boyles RA (1983) On the convergence of the em algorithm. *Journal of the Royal Statistical Society: Series B (Methodological)* 45(1):47–50
- Cappé O, Moulines E (2009) On-line expectation-maximization algorithm for latent data models. *Journal of the Royal Statistical Society: Series B (Statistical Methodology)* 71(3):593–613
- Chen HF, Guo L, Gao AJ (1987) Convergence and robustness of the robbins-monro algorithm truncated at randomly varying bounds. *Stochastic Processes and their Applications* 27:217–231
- Chen J, Zhu J, Teh YW, Zhang T (2018) Stochastic expectation maximization with variance reduction. *Advances in Neural Information Processing Systems* 31:7967–7977
- Delyon B, Lavielle M, Moulines E, et al. (1999) Convergence of a stochastic approximation version of the em algorithm. *The Annals of Statistics* 27(1):94–128
- Dempster AP, Laird NM, Rubin DB (1977) Maximum likelihood from incomplete data via the em algorithm. *Journal of the Royal Statistical Society: Series B (Methodological)* 39(1):1–22
- Dwivedi R, Ho N, Khamaru K, Jordan MI, Wainwright MJ, Yu B (2018) Singularity, misspecification, and the convergence rate of em. *arXiv preprint arXiv:181000828*
- Dwivedi R, Ho N, Khamaru K, Wainwright M, Jordan M, Yu B (2020) Sharp analysis of expectation-maximization for weakly identifiable models. In: *International Conference on Artificial Intelligence and Statistics*, PMLR, pp 1866–1876
- Fort G, Moulines E (2003) Convergence of the monte carlo expectation maximization for curved exponential families. *The Annals of Statistics* 31(4):1220–1259
- Fort G, Moulines E, Wai HT (2020) A stochastic path integral differential estimator expectation maximization algorithm. *Advances in Neural Information Processing Systems* 33
- Geyer CJ, Thompson EA (1995) Annealing markov chain monte carlo with applications to ancestral inference. *Journal of the American Statistical Association* 90(431):909–920
- Ho N, Nguyen X, et al. (2016) Convergence rates of parameter estimation for some weakly identifiable finite mixtures. *The Annals of Statistics* 44(6):2726–2755
- Hukushima K, Nemoto K (1996) Exchange monte carlo method and application to spin glass simulations. *Journal of the Physical Society of Japan* 65(6):1604–1608
- Jank W (2005) Quasi-monte carlo sampling to improve the efficiency of monte carlo em. *Computational statistics & data analysis* 48(4):685–701
- Karimi B, Wai HT, Moulines E, Lavielle M (2019) On the global convergence of (fast) incremental expectation maximization methods. In: *Advances in Neural Information Processing Systems*, pp 2837–2847
- Kirkpatrick S, Gelatt CD, Vecchi MP (1983) Optimization by simulated annealing. *science* 220(4598):671–680
- Kuhn E, Lavielle M (2005) Maximum likelihood estimation in nonlinear mixed effects models. *Computational Statistics & Data Analysis* 49(4):1020–1038

- Lange K (1995) A gradient algorithm locally equivalent to the em algorithm. *Journal of the Royal Statistical Society: Series B (Methodological)* 57(2):425–437
- Levine RA, Casella G (2001) Implementations of the monte carlo em algorithm. *Journal of Computational and Graphical Statistics* 10(3):422–439
- Levine RA, Fan J (2004) An automated (markov chain) monte carlo em algorithm. *Journal of Statistical Computation and Simulation* 74(5):349–360
- Naim I, Gildea D (2012) Convergence of the em algorithm for gaussian mixtures with unbalanced mixing coefficients. *arXiv preprint arXiv:12066427*
- Neal RM, Hinton GE (1998) A view of the em algorithm that justifies incremental, sparse, and other variants. In: *Learning in graphical models*, Springer, pp 355–368
- Ng SK, McLachlan GJ (2003) On the choice of the number of blocks with the incremental em algorithm for the fitting of normal mixtures. *Statistics and Computing* 13(1):45–55
- Pan JX, Thompson R (1998) Quasi-monte carlo em algorithm for mles in generalized linear mixed models. In: *COMPSTAT*, Springer, pp 419–424
- Swendsen RH, Wang JS (1986) Replica monte carlo simulation of spin-glasses. *Physical review letters* 57(21):2607
- Titterton D, Smith A, Makov U (1985) *Statistical Analysis of Finite Mixture Distributions*. Wiley, New York
- Ueda N, Nakano R (1998) Deterministic annealing em algorithm. *Neural networks* 11(2):271–282
- Van Laarhoven PJ, Aarts EH (1987) Simulated annealing. In: *Simulated annealing: Theory and applications*, Springer, pp 7–15
- Wei GC, Tanner MA (1990) A monte carlo implementation of the em algorithm and the poor man’s data augmentation algorithms. *Journal of the American statistical Association* 85(411):699–704
- Winkelbauer A (2012) Moments and absolute moments of the normal distribution. *arXiv preprint arXiv:12094340*
- Wu CJ (1983) On the convergence properties of the em algorithm. *The Annals of statistics* 11(1):95–103

Supplements to: Deterministic Approximate EM algorithm

Application to the Riemann approximation EM and the tempered EM

Thomas Lartigue · Stanley Durrleman ·
Stéphanie Allasonnière

the date of receipt and acceptance should be inserted later

1 Introduction

In these supplementary materials, we give in full details the proofs that were sketched in the main paper detail and a more extensive experimental study of the tempered EM algorithm (tmp-EM). Section 2 is dedicated to the proofs. Section 2.1 details the proof of convergence for the Deterministic Approximate EM algorithm, our central result, Theorem ?? of the paper. Section 2.2 details the proof of convergence for tmp-EM, Theorem ?? of the paper. In Section 3, we perform an in depth experimental study of the behaviour and performances of tmp-EM to demonstrate that it solves the issues raised about the EM. In particular, we illustrate on synthetic data, in the GMM case, that tmp-EM consistently reaches better values of the likelihood than the unmodified EM, in addition to better estimating the GMM parameters. We demonstrate that, as intended, tmp-EM is able to escape bad initialisations, unlike EM, and that more diverse configurations are explored during the procedure before reaching convergence. We confirm these observation on real data from the scikit learn library [6]. Finally, in Section 4, we test the tmp-EM within a more complex pipeline: the Independent Factor Analysis model [3] with a hidden GMM. We illustrate that, with tmp-EM, the identified sources are cleaner, more stable looking, and closer to the real ones when those are known.

T. Lartigue
Aramis project-team, Inria and CMAP, CNRS, École polytechnique, I.P. Paris
E-mail: thomas.lartigue@inria.fr
Present address: thomas.lartigue@dzne.de

S. Durrleman
Aramis project-team, Inria
E-mail: stanley.durrleman@fr

S. Allasonnière
Centre de Recherche des Cordeliers, Université de Paris, INSERM, Sorbonne Université
E-mail: stephanie.allasonniere@parisdescartes.fr

2 Proofs of the two main Theorems

2.1 Proof of the general theorem

In this Section, we prove Theorem ?? of the main paper, for the convergence of the Deterministic Approximate EM algorithm.

We use two intermediary results of [5]: their “Proposition 9” and “Proposition 11”, which we recall here:

Proposition 1 (“Proposition 9”) *Let $\Theta \subseteq \mathbb{R}^l$, K compact $\subset \Theta$, $\mathcal{L} \subseteq \Theta$ such that $\mathcal{L} \cap K$ compact. Let us assume*

- WC^0 Lyapunov function with regards to (T, \mathcal{L}) .
- $\exists u_n \in K^{\mathbb{N}}$ such that $|W(u_{n+1}) - W \circ T(u_n)| \xrightarrow[n \rightarrow \infty]{} 0$

Then

- $\{W(u_n)\}_{n \in \mathbb{N}}$ converges towards a connected component of $W(\mathcal{L} \cap K)$
- If $W(\mathcal{L} \cap K)$ has an empty interior, then $\{W(u_n)\}_n$ converges towards w^* and $\{u_n\}_n$ converges towards the set $\mathcal{L}_{w^*} \cap K$

$$\mathcal{L}_{w^*} = \{\theta \in \mathcal{L} | W(\theta) = w^*\}$$

Proposition 2 (“Proposition 11”) *Let $\Theta \subseteq \mathbb{R}^l$, T and $\{F_n\}_n$ point to point maps on Θ . Let $\{\theta_n\}_n$ be the sequence defined by the stable approximate EM with likelihood f and approximate maps sequence $\{F_n\}_n$. Let $\mathcal{L} \subset \Theta$. We assume*

- the A1 – 2 conditions of Proposition 10 of [5].
- **(A1)** There exists W , a C^0 Lyapunov function with regards to (T, \mathcal{L}) such that $\forall M > 0$, $\{\theta \in \Theta, W(\theta) > M\}$ is compact, and:

$$\Theta = \bigcup_{n \in \mathbb{N}} \left\{ \theta \in \Theta | W(\theta) > n^{-1} \right\}.$$

- **(A2)** $W(\mathcal{L})$ is compact OR **(A2’)** $W(\mathcal{L} \cap K)$ is finite for all compact $K \subseteq \Theta$.
- $\forall u \in K_0$, $\lim_{n \rightarrow \infty} |W \circ F_n - W \circ T|(u) = 0$
- \forall compact $K \subseteq \Theta$, $\lim_{n \rightarrow \infty} |W \circ F_n(u_n) - W \circ T(u_n)| \mathbb{1}_{u_n \in K} = 0$

Then

With probability 1, $\limsup_{n \rightarrow \infty} p_n < \infty$ and $\{u_n\}_n$ compact sequence

Remark 1 In [5], condition **(A1)** is mistakenly written as:

$$\Theta = \bigcup_{n \in \mathbb{N}} \{\theta \in \Theta | W(\theta) > n\}.$$

This is a typo that we have corrected here.

We need to prove that, under the conditions of Theorem ??, we verify the conditions of Proposition Proposition 1 and Proposition 2. Then we will have the results announced in Theorem ??.

2.1.1 Verifying the conditions of 2

f is the likelihood function of a model of the curved exponential family. \mathcal{L} the set of its critical points: $\mathcal{L} := \{\theta \in \Theta | \nabla f(\theta) = 0\}$. Let T be the point to point map describing the transition between θ_n and θ_{n+1} in the exact EM algorithm. The general properties of the EM tell us that its stationary points are the critical points of f : $\mathcal{L} = \{\theta \in \Theta | T(\theta) = \theta\}$. Additionally, f is a C^0 Lyapunov function associated to (T, \mathcal{L}) . Let $\{\theta_n\}_n$ be the sequence defined by the stable approximate EM with $\{F_n\}_{n \in \mathbb{N}}$ our sequence of point to point maps.

We verify that under this framework - and with the assumptions of Theorem ?? - we check the conditions of Proposition 2.

As in [5], $M1 - 3$ implies $A1 - 2$.

Let us show that we have the last two conditions for Proposition 2:

$$\forall \theta \in K_0, \quad \lim_{n \rightarrow \infty} |f \circ F_n - f \circ T|(\theta) = 0, \quad (1)$$

and

$$\forall \text{ compact } K \subseteq \Theta, \quad \lim_{n \rightarrow \infty} |f \circ F_n(\theta_n) - f \circ T(\theta_n)| \mathbb{1}_{\theta_n \in K} = 0. \quad (2)$$

We focus on (2), since (1) is easier to verify and will come from the same reasoning. The first steps are similar to [5]. We underline the most consequent deviations from the proof of [5] when they occur.

Equivalent formulation of the convergence We write Eq. (2) under an equivalent form. First note that $F_n(\theta_n) = \hat{\theta}(\tilde{S}_n(\theta_n))$ and $T(\theta_n) = \hat{\theta}(\bar{S}(\theta_n))$. Hence $|f \circ F_n(u_n) - f \circ T(u_n)| = |f \circ \hat{\theta}(\tilde{S}_n(\theta_n)) - f \circ \hat{\theta}(\bar{S}(\theta_n))|$. To show Eq. (2):

$$|f \circ \hat{\theta}(\tilde{S}_n(\theta_n)) - f \circ \hat{\theta}(\bar{S}(\theta_n))| \mathbb{1}_{\theta_n \in K} \xrightarrow{n \rightarrow \infty} 0,$$

it is sufficient and necessary to have:

$$\forall \epsilon > 0, \exists N \in \mathbb{N}, \forall n \geq N, |f \circ \hat{\theta}(\tilde{S}_n(\theta_n)) - f \circ \hat{\theta}(\bar{S}(\theta_n))| \mathbb{1}_{\theta_n \in K} \leq \epsilon.$$

An other equivalent formulation is that there are a finite number of integers n such that $|f \circ \hat{\theta}(\tilde{S}_n(\theta_n)) - f \circ \hat{\theta}(\bar{S}(\theta_n))| \mathbb{1}_{\theta_n \in K} > \epsilon$, in other words:

$$\forall \epsilon > 0, \sum_{n=1}^{\infty} \mathbb{1}_{|f \circ \hat{\theta}(\tilde{S}_n(\theta_n)) - f \circ \hat{\theta}(\bar{S}(\theta_n))| \mathbb{1}_{\theta_n \in K} > \epsilon} < \infty.$$

Use the uniform continuity We aim to relate the proximity between the images $f \circ \hat{\theta}$ of to the proximity between the antecedents of $f \circ \hat{\theta}$. The function $f \circ \hat{\theta} : \mathbb{R}^q \rightarrow \mathbb{R}$ is continuous, but not necessarily uniformly continuous on \mathbb{R}^q . As a consequence, we will need to restrict ourselves to a compact to get uniform continuity properties. We already have a given compact K . $\tilde{S} : \Theta \rightarrow \mathbb{R}^l$ is continuous, hence $S(K)$ is a compact as well. Let δ be a strictly positive real number. Let $\bar{S}(K, \delta) := \left\{ s \in \mathbb{R}^q \left| \inf_{t \in K} \|\bar{S}(t) - s\| \leq \delta \right. \right\}$. Where we use any norm $\|\cdot\|$ on \mathbb{R}^q since they are all

equivalent. $\bar{S}(K, \delta)$ is a compact set as well. As a consequence $f \circ \theta$ is uniformly continuous on $\bar{S}(K, \delta)$, which means that:

$$\forall \epsilon > 0, \exists \eta(\epsilon, \delta) > 0, \forall x, y \in \bar{S}(K, \delta), \|x - y\| \leq \eta(\epsilon, \delta) \implies |f \circ \hat{\theta}(x) - f \circ \hat{\theta}(y)| \leq \epsilon. \quad (3)$$

Let us show that, with $\alpha := \min(\delta, \eta(\epsilon, \delta))$, $\forall n$,

$$|f \circ \hat{\theta}(\tilde{S}_n(\theta_n)) - f \circ \hat{\theta}(\bar{S}(\theta_n))| \mathbb{1}_{\theta_n \in K} > \epsilon \implies \|\tilde{S}_n(\theta_n) - \bar{S}(\theta_n)\| \mathbb{1}_{\theta_n \in K} > \alpha. \quad (4)$$

To that end, we show that:

$$\|\tilde{S}_n(\theta_n) - \bar{S}(\theta_n)\| \mathbb{1}_{\theta_n \in K} \leq \alpha \implies |f \circ \hat{\theta}(\tilde{S}_n(\theta_n)) - f \circ \hat{\theta}(\bar{S}(\theta_n))| \mathbb{1}_{\theta_n \in K} \leq \epsilon.$$

Let us assume that $\|\tilde{S}_n(\theta_n) - \bar{S}(\theta_n)\| \mathbb{1}_{\theta_n \in K} \leq \alpha$.

If $\theta_n \notin K$, then $|f \circ \hat{\theta}(\tilde{S}_n(\theta_n)) - f \circ \hat{\theta}(\bar{S}(\theta_n))| \mathbb{1}_{\theta_n \in K} = 0 \leq \epsilon$.

If, in contrary, $\theta_n \in K$, then $\bar{S}(\theta_n) \in \bar{S}(K) \subset \bar{S}(K, \delta)$. Since $\|\tilde{S}_n(\theta_n) - \bar{S}(\theta_n)\| = \|\tilde{S}_n(\theta_n) - \bar{S}(\theta_n)\| \mathbb{1}_{\theta_n \in K} \leq \alpha \leq \delta$, then $\tilde{S}_n(\theta_n) \in \bar{S}(K, \delta)$. Since $(\bar{S}(\theta_n), \tilde{S}_n(\theta_n)) \in \bar{S}(K, \delta)^2$ and $\|\tilde{S}_n(\theta_n) - \bar{S}(\theta_n)\| \leq \alpha \leq \eta(\epsilon, \delta)$, then we get from Eq. (3)

$$|f \circ \hat{\theta}(\tilde{S}_n(\theta_n)) - f \circ \hat{\theta}(\bar{S}(\theta_n))| \mathbb{1}_{\theta_n \in K} \leq \epsilon.$$

In both cases, we get that:

$$\|\tilde{S}_n(\theta_n) - \bar{S}(\theta_n)\| \mathbb{1}_{\theta_n \in K} \leq \alpha \implies |f \circ \hat{\theta}(\tilde{S}_n(\theta_n)) - f \circ \hat{\theta}(\bar{S}(\theta_n))| \mathbb{1}_{\theta_n \in K} \leq \epsilon,$$

which proves Eq. (4).

Sufficient condition for convergence We use Eq. (4) to find a sufficient condition for (2). This part differs from [5] as our approximation is not defined as a random sum. Eq. (4) is equivalent to

$$\mathbb{1}_{|f \circ \hat{\theta}(\tilde{S}_n(\theta_n)) - f \circ \hat{\theta}(\bar{S}(\theta_n))| \mathbb{1}_{\theta_n \in K} > \epsilon} \leq \mathbb{1}_{\|\tilde{S}_n(\theta_n) - \bar{S}(\theta_n)\| \mathbb{1}_{\theta_n \in K} > \alpha}.$$

From that, we get

$$\forall \epsilon > 0, \exists \alpha > 0 \sum_{n=1}^{\infty} \mathbb{1}_{|f \circ \hat{\theta}(\tilde{S}_n(\theta_n)) - f \circ \hat{\theta}(\bar{S}(\theta_n))| \mathbb{1}_{\theta_n \in K} > \epsilon} \leq \sum_{n=1}^{\infty} \mathbb{1}_{\|\tilde{S}_n(\theta_n) - \bar{S}(\theta_n)\| \mathbb{1}_{\theta_n \in K} > \alpha}.$$

As a consequence, if

$$\forall \alpha > 0, \sum_{n=1}^{\infty} \mathbb{1}_{\|\tilde{S}_n(\theta_n) - \bar{S}(\theta_n)\| \mathbb{1}_{\theta_n \in K} > \alpha} < \infty$$

Then

$$\forall \epsilon > 0, \sum_{n=1}^{\infty} \mathbb{1}_{|f \circ \hat{\theta}(\tilde{S}_n(\theta_n)) - f \circ \hat{\theta}(\bar{S}(\theta_n))| \mathbb{1}_{\theta_n \in K} > \epsilon} < \infty$$

In other, equivalent, words:

$$\begin{aligned} \text{If } \quad & \|\tilde{S}_n(\theta_n) - \bar{S}(\theta_n)\| \mathbb{1}_{\theta_n \in K} \xrightarrow{n \rightarrow \infty} 0 \\ \text{Then } & |f \circ \hat{\theta}(\tilde{S}_n(\theta_n)) - f \circ \hat{\theta}(\bar{S}(\theta_n))| \mathbb{1}_{\theta_n \in K} \xrightarrow{n \rightarrow \infty} 0. \end{aligned} \quad (5)$$

Hence, having for all compact sets $K \subset \Theta$, $\|\tilde{S}_n(\theta_n) - \bar{S}(\theta_n)\| \mathbb{1}_{\theta_n \in K} \xrightarrow[n \rightarrow \infty]{} 0$ is sufficient to have the desired condition (2). Similarly, we find that $\forall \theta \in K_0$:

$$\begin{aligned} & \|\tilde{S}_n(\theta) - \bar{S}(\theta)\| \xrightarrow[n \rightarrow \infty]{} 0 \\ \implies & |f \circ \hat{\theta}(\tilde{S}_n(\theta)) - f \circ \hat{\theta}(\bar{S}(\theta))| \xrightarrow[n \rightarrow \infty]{} 0, \end{aligned} \quad (6)$$

which gives us a sufficient condition for (1).

Further simplifications of the desired result with successive sufficient conditions We find another, simpler, sufficient condition for (2) from Eq. (5). This part is unique to our proof and absent from [5]. It is here that we relate the formal conditions of Proposition ?? to the specific assumptions of our Theorem ??.

We first remove the dependency on the terms $\{\theta_n\}_n$ of the EM sequence:

$$\|\tilde{S}_n(\theta_n) - \bar{S}(\theta_n)\| \mathbb{1}_{\theta_n \in K} \leq \sup_{\theta \in K} \|\tilde{S}_n(\theta) - \bar{S}(\theta)\|. \quad (7)$$

From Eq. (5), (6) and (7) we get that:

$$\forall \text{ compact } K \subset \Theta, \quad \sup_{\theta \in K} \|\tilde{S}_n(\theta) - \bar{S}(\theta)\| \xrightarrow[n \rightarrow \infty]{} 0,$$

is a sufficient condition to have both Eq. (1) and (2).

To show that the hypotheses of Theorem ?? imply this sufficient condition, we express it in integral form. Let $S = \{S_u\}_{u=1, \dots, q}$. We recall that $\tilde{S}_n(\theta) = \{\int_z S_u(z) \tilde{p}_{\theta, n}(z) dz\}_i$ and $\bar{S}(\theta) = \{\int_z S_u(z) p_\theta(z) dz\}_u$. Hence:

$$\tilde{S}_n(\theta) - \bar{S}(\theta) = \left\{ \int_z S_u(z) (\tilde{p}_{\theta, n}(z) - p_\theta(z)) dz \right\}_u.$$

These q terms can be upper bounded by two different terms depending on the existence of the involved quantities:

$$\int_z S_u(z) (\tilde{p}_{\theta, n}(z) - p_\theta(z)) dz \leq \left(\int_z S_u(z)^2 dz \right)^{\frac{1}{2}} \left(\int_z (\tilde{p}_{\theta, n}(z) - p_\theta(z))^2 dz \right)^{\frac{1}{2}},$$

and

$$\int_z S_u(z) (\tilde{p}_{\theta, n}(z) - p_\theta(z)) dz \leq \left(\int_z S_u(z)^2 p_\theta(z) dz \right)^{\frac{1}{2}} \left(\int_z \left(\frac{\tilde{p}_{\theta, n}(z)}{p_\theta(z)} - 1 \right)^2 p_\theta(z) dz \right)^{\frac{1}{2}}.$$

As a consequence, if $\int_z S_u(z)^2 dz$ exists, then it is sufficient to show have:

$$\sup_{\theta \in K} \int_z (\tilde{p}_{\theta, n}(z) - p_\theta(z))^2 dz \xrightarrow[n \rightarrow \infty]{} 0,$$

and if $\int_z S_u(z)^2 p_\theta(z) dz$ exists, then it is sufficient to show have:

$$\sup_{\theta \in K} \int_z \left(\frac{\tilde{p}_{\theta, n}(z)}{p_\theta(z)} - 1 \right)^2 p_\theta(z) dz \xrightarrow[n \rightarrow \infty]{} 0.$$

Among the assumptions of Theorem ?? is one that states that for all compacts $K \subseteq \Theta$, one of those scenarios has to be true. Hence our sufficient condition is met.

Conclusion With the hypothesis of Theorem ??, we have

$$\forall \text{ compact } K \subseteq \Theta, \quad \sup_{\theta \in K} \|\tilde{S}_n(\theta) - \bar{S}(\theta)\| \xrightarrow{n \rightarrow \infty} 0,$$

which is a sufficient condition to verify both Eq. (1) and (2). With these two conditions, we can apply Proposition 2.

2.1.2 Applying 2

Since we verify all the conditions of Proposition 2, we can apply its conclusions:

With probability 1, $\limsup_{n \rightarrow \infty} p_n < \infty$ and $\{\theta_n\}_n$ compact sequence ,

which is specifically the result (i)(a) of Theorem ??.

2.1.3 Verifying the conditions of 1

With Proposition 1, we prove the remaining points of Theorem ??: (i)(b) and (ii).

For the application of Proposition 1:

- $Cl(\{\theta_n\}_n)$ plays the part of the compact K
- $\{\theta \in \Theta | \nabla f(\theta) = 0\} = \{\theta \in \Theta | T(\theta) = \theta\}$ plays the part of the set \mathcal{L}
- The likelihood f is the C^0 Lyapunov function with regards to (T, \mathcal{L})
- $\{\theta_n\}_n$ is the K valued sequence (since K is $Cl(\{\theta_n\}_n)$).

The last condition that remains to be shown to apply Proposition 1 is that:

$$\lim_{n \rightarrow \infty} |f(\theta_{n+1}) - f \circ T(\theta_n)| = 0.$$

We have more or less already proven that, in the previous section of the Proof, with $F_n(\theta_n)$ in place of θ_{n+1} . The only indices where $F_n(\theta_n) \neq \theta_{n+1}$ are when the value of the sequence p_n experiences an increment of 1. We have proven with Proposition 2 that there is only a finite number of such increments.

$$|f(\theta_{n+1}) - f \circ T(\theta_n)| = |f(\theta_0) - f \circ T(\theta_n)| \mathbb{1}_{p_{n+1}=p_n+1} + |f \circ F_n(\theta_n) - f \circ T(\theta_n)| \mathbb{1}_{p_{n+1}=p_n}.$$

Since there is only a finite number of increments of the value of p_n , then $\exists N \in \mathbb{N}, \forall n \geq N, \mathbb{1}_{p_{n+1}=p_n+1} = 0$ and $\mathbb{1}_{p_{n+1}=p_n} = 1$. In other words:

$$\begin{aligned} \exists N \in \mathbb{N}, \forall n \geq N, \quad |f(\theta_{n+1}) - f \circ T(\theta_n)| &= |f \circ F_n(\theta_n) - f \circ T(\theta_n)| \\ \exists N \in \mathbb{N}, \forall n \geq N, \quad |f(\theta_{n+1}) - f \circ T(\theta_n)| &= |f \circ F_n(\theta_n) - f \circ T(\theta_n)| \mathbb{1}_{\theta_n \in Cl(\{\theta_k\}_k)}. \end{aligned}$$

Since θ_n is always in $Cl(\{\theta_k\}_k)$ by definition. Additionally Proposition 2 tells us that $Cl(\{\theta_k\}_k)$ is a compact. Moreover, in order to use Proposition 2 in the first place, we had proven that:

$$\forall \text{ compact } K \subseteq \Theta, \quad \lim_{n \rightarrow \infty} |f \circ F_n(\theta_n) - f \circ T(\theta_n)| \mathbb{1}_{\theta_n \in K} = 0.$$

We can apply this directly with $K = Cl(\{\theta_k\}_k)$ to conclude the desired result:

$$\lim_{n \rightarrow \infty} |f(\theta_{n+1}) - f \circ T(\theta_n)| = 0$$

Hence we verify all the conditions to apply Proposition 1.

2.1.4 Applying 1

Since we verify all we need, we have the conclusions of Proposition 1:

- $\{f(\theta_n)\}_{n \in \mathbb{N}}$ converges towards a connected component of $f(\mathcal{L} \cap Cl(\{\theta_n\}_n)) \subset f(\mathcal{L})$
- If $f(\mathcal{L} \cap Cl(\{\theta_n\}_n))$ has an empty interior, then $\{f(\theta_n)\}_{n \in \mathbb{N}}$ converges towards a $f^* \in \mathbb{R}$ and $\{\theta_n\}_n$ converges towards $\mathcal{L}_{f^*} \cap Cl(\{\theta_n\}_n)$. Where $\mathcal{L}_{f^*} := \{\theta \in \mathcal{L} | f(\theta) = f^*\}$

Both points are respectively the statements (i)(b) and (ii) of Theorem ??.
Which concludes the proof of the Theorem.

2.2 Proof of the tempering theorem

In this Section, we prove Theorem ?? of the main paper, the convergence of the tempered EM algorithm. For that, we need to show that we verify each of the hypothesis of the more general Theorem ??.

We already assumed the conditions M1, M2 and M3 in the hypothesis of Theorem

?. To apply Theorem ??, we need to show that when $\tilde{p}_{\theta,n}(z) := \frac{p_{\theta}^{\frac{1}{T_n}}(z)}{\int_{z'} p_{\theta}^{\frac{1}{T_n}}(z') dz'}$, then \forall compact $K \subseteq \Theta$, one of the two following configurations holds:

$$\int_z S(z)^2 dz < \infty \text{ and } \sup_{\theta \in K} \int_z (\tilde{p}_{\theta,n}(z) - p_{\theta}(z))^2 dz \xrightarrow{n \rightarrow \infty} 0,$$

or

$$\sup_{\theta \in K} \int_z S(z)^2 p_{\theta}(z) dz < \infty \text{ and } \sup_{\theta \in K} \int_z \left(\frac{\tilde{p}_{\theta,n}(z)}{p_{\theta}(z)} - 1 \right)^2 p_{\theta}(z) dz \xrightarrow{n \rightarrow \infty} 0.$$

Since we have assumed:

$$\forall \text{ compact } K \in \Theta, \forall \alpha \in \overline{B}(1, \epsilon), \forall u, \quad \sup_{\theta \in K} \int_z S_u^2(z) p_{\theta}^{\alpha}(z) dz < \infty,$$

then we already verify the first half of the second configuration for all the compacts K . Hence it is sufficient to prove that:

$$\forall \text{ compact } K \in \Theta, \quad \sup_{\theta \in K} \int_z \left(\frac{\tilde{p}_{\theta,n}(z)}{p_{\theta}(z)} - 1 \right)^2 p_{\theta}(z) dz \xrightarrow{n \rightarrow \infty} 0, \quad (8)$$

to have the desired result. The rest of the proof is dedicated to this goal.

2.2.1 Taylor development

We use the Taylor's formula of the first order with the mean-value form of the reminder. For a derivable function g :

$$g(x) = g(0) + g'(a)x, \quad a \in [0, x], \quad (9)$$

where the interval $[0, x]$ has a flexible meaning since x could be negative.
We apply it to:

$$g(x) = e^x, \quad g'(x) = e^x, \quad g(x) = 1 + xe^a, \quad a \in [0, x],$$

and:

$$g(x) = \frac{1}{1+x}, \quad g'(x) = -\frac{1}{(1+x)^2}, \quad g(x) = 1 - \frac{x}{(1+a)^2}, \quad a \in [0, x].$$

To make the upcoming calculation more readable, we momentarily replace $p_\theta(z)$ by simply p and T_n by T .

$$\begin{aligned} p^{\frac{1}{T}} &= p \left(p^{\frac{1}{T}-1} \right) \\ &= p e^{(\frac{1}{T}-1) \ln p} \\ &= p + \left(\frac{1}{T} - 1 \right) p \ln p e^a, \quad a \in \left[0, \left(\frac{1}{T} - 1 \right) \ln p \right], \end{aligned}$$

where $a = a(z, \theta, T_n)$ since it depends on the value of $p_\theta(z)$ and T_n . Provided that the following quantities are defined, we have:

$$\int_z p^{\frac{1}{T}} = 1 + \left(\frac{1}{T} - 1 \right) \int_z p \ln p e^a,$$

Hence:

$$\frac{1}{\int_z p^{\frac{1}{T}}} = 1 - \left(\frac{1}{T} - 1 \right) \frac{\int_z p \ln p e^a}{(1+b)^2}, \quad b \in \left[0, \left(\frac{1}{T} - 1 \right) \int_z p \ln p e^a \right],$$

where $b = b(\theta, T_n)$ since it depends on the value of T_n the integral over z of a function of z and θ .

In the end, we have:

$$\frac{p^{\frac{1}{T}}}{\int_z p^{\frac{1}{T}}} = p + \left(\frac{1}{T} - 1 \right) p \ln p e^a \left(1 - \left(\frac{1}{T} - 1 \right) \frac{\int_z p \ln p e^a}{(1+b)^2} \right) - \left(\frac{1}{T} - 1 \right) p \frac{\int_z p \ln p e^a}{(1+b)^2}. \quad (10)$$

Since for any real numbers $(x+y)^2 \leq 2(x^2+y^2)$, then:

$$\begin{aligned} \left(\frac{p^{\frac{1}{T}}}{\int_z p^{\frac{1}{T}}} - p \right)^2 &\leq 2 \left(\frac{1}{T} - 1 \right)^2 p^2 \left((\ln p e^a)^2 \left(1 - \left(\frac{1}{T} - 1 \right) \frac{\int_z p \ln p e^a}{(1+b)^2} \right)^2 + \left(\frac{\int_z p \ln p e^a}{(1+b)^2} \right)^2 \right) \\ &= 2 \left(\frac{1}{T} - 1 \right)^2 p^2 \left((\ln p e^a)^2 A + B \right). \end{aligned}$$

where $A = A(\theta, T_n)$ and $B = B(\theta, T_n)$. So far the only condition that has to be verified for all the involved quantities to be defined is that $\int_z p \ln p e^a$ exists. With this Taylor development on hand, we state, prove and apply two lemmas which allow us to get (8) and conclude the proof of the theorem.

2.2.2 Two intermediary lemmas

The two following lemmas provides every result we need to finish the proof.

Lemma 1 *With*

$$p_\theta(z) = \exp(\psi(\theta) + \langle S(z), \phi(\theta) \rangle),$$

then

$$\int_z p_\theta^\alpha(z) \ln^2 p_\theta(z) dz \leq 2\psi(\theta)^2 \int_z p_\theta^\alpha(z) dz + 2 \|\phi(\theta)\|^2 \cdot \sum_u \int_z S_u^2(z) p_\theta^\alpha(z).$$

and

$$\int_z p_\theta^\alpha(z) |\ln p_\theta(z)| dz \leq |\psi(\theta)| \int_z p_\theta^\alpha(z) dz + \|\phi(\theta)\| \cdot \left(\sum_u \int_z S_u^2(z) p_\theta^\alpha(z) \int_z p_\theta^\alpha(z) \right)^{\frac{1}{2}}.$$

Proof For the first inequality, using the fact that $(a + b)^2 \leq 2(a^2 + b^2)$, we have:

$$\int_z p_\theta^\alpha(z) \ln^2 p_\theta(z) dz \leq 2\psi(\theta)^2 \int_z p_\theta^\alpha(z) dz + 2 \int_z p_\theta^\alpha(z) \langle S(z), \phi(\theta) \rangle^2,$$

We use Cauchy-Schwartz:

$$\langle S(z), \phi(\theta) \rangle^2 \leq \|\phi\|^2 \|S(z)\|^2 = \|\phi\|^2 \sum_u S_u(z)^2,$$

to get the desired result:

$$\int_z p_\theta^\alpha(z) \ln^2 p_\theta(z) dz \leq 2\psi(\theta)^2 \int_z p_\theta^\alpha(z) dz + 2 \|\phi(\theta)\|^2 \cdot \sum_u \int_z S_u^2(z) p_\theta^\alpha(z).$$

For the second inequality, we start with Cauchy-Schwartz on $\langle \int_z S(z) p_\theta^\alpha(z), \phi(\theta) \rangle$:

$$\int_z p_\theta^\alpha(z) |\ln p_\theta(z)| dz \leq |\psi(\theta)| \int_z p_\theta^\alpha(z) dz + \|\phi(\theta)\| \cdot \left\| \int_z S(z) p_\theta^\alpha(z) \right\|.$$

Moreover, since:

$$\int_z S_u(z) p_\theta^\alpha(z) dz \leq \left(\int_z S_u^2(z) p_\theta^\alpha(z) dz \right)^{\frac{1}{2}} \left(\int_z p_\theta^\alpha(z) dz \right)^{\frac{1}{2}},$$

then

$$\int_z p_\theta^\alpha(z) |\ln p_\theta(z)| dz \leq |\psi(\theta)| \int_z p_\theta^\alpha(z) dz + \|\phi(\theta)\| \cdot \left(\sum_u \int_z S_u^2(z) p_\theta^\alpha(z) \int_z p_\theta^\alpha(z) \right)^{\frac{1}{2}}.$$

Lemma 2 *With K compact and $\epsilon \in \mathbb{R}_+^*$,*

$$p_\theta(z) = \exp(\psi(\theta) + \langle S(z), \phi(\theta) \rangle),$$

and

$$\tilde{p}_{\theta,n}(z) := \frac{p_\theta^{\frac{1}{T_n}}(z)}{\int_{z'} p_\theta^{\frac{1}{T_n}}(z') dz'},$$

if

- (i) $T_n \in \mathbb{R}_+^* \xrightarrow{n \rightarrow \infty} 1$,
- (ii) $\sup_{\theta \in K} \psi(\theta) < \infty$,
- (iii) $\sup_{\theta \in K} \|\phi(\theta)\| < \infty$,
- (iv) $\forall \alpha \in \bar{B}(1, \epsilon), \sup_{\theta \in K} \int_z p_\theta^\alpha(z) dz < \infty$,
- (v) $\forall \alpha \in \bar{B}(1, \epsilon), \forall u, \sup_{\theta \in K} \int_z S_u^2(z) p_\theta^\alpha(z) dz < \infty$.

then

$$\sup_{\theta \in K} \int_z \left(\frac{\tilde{p}_{\theta, n}(z)}{p_\theta(z)} - 1 \right)^2 p_\theta(z) dz \xrightarrow{n \rightarrow \infty} 0 .$$

Proof Provided that the following integrals exist, we have, thanks to the Taylor development:

$$\begin{aligned} \int_z \frac{1}{p} \left(\frac{p^{\frac{1}{T}}}{\int_z p^{\frac{1}{T}}} - p \right)^2 &\leq 2 \int_z \left(\frac{1}{T} - 1 \right)^2 p \left((\ln p e^a)^2 A + B \right) \\ &= 2 \left(\frac{1}{T} - 1 \right)^2 A \int_z p e^{2a} \ln^2 p + 2 \left(\frac{1}{T} - 1 \right)^2 B . \end{aligned} \quad (11)$$

In this proof, we find finite upper bounds independent of θ and T_n for $A(\theta, T_n)$, $B(\theta, T_n)$ and $\int_z p e^{2a} \ln^2 p$, then - since $\left(\frac{1}{T_n} - 1 \right) \rightarrow 0$ - we have the desired result.

We start by studying $A(\theta, T_n) = \left(1 - \left(\frac{1}{T} - 1 \right) \frac{\int_z p \ln p e^a}{(1+b)^2} \right)^2$. The first term of interest here is $\int_z p \ln p e^a$. We have:

$$\begin{aligned} a &\in \left[0, \left(\frac{1}{T} - 1 \right) \ln p \right] , \\ e^a &\in \left[1, p^{\frac{1}{T}-1} \right] , \\ p \ln p e^a &\in \left[p \ln p, p^{\frac{1}{T}} \ln p \right] . \end{aligned}$$

where we recall that the interval is to be taken in a flexible sense, since we do not now a priori which bound is the largest and which is the smallest. What we have without doubt though is:

$$|p \ln p e^a| \leq \max \left(|p \ln p|, \left| p^{\frac{1}{T}} \ln p \right| \right) .$$

We find an upper bound on both those term. Let $\alpha \in \bar{B}(1, \epsilon)$, the second result of Lemma 1 gives us:

$$\int_z p_\theta^\alpha(z) |\ln p_\theta(z)| dz \leq |\psi(\theta)| \int_z p_\theta^\alpha(z) dz + \|\phi(\theta)\| \cdot \left(\sum_u \int_z S_u^2(z) p_\theta^\alpha(z) \int_z p_\theta^\alpha(z) \right)^{\frac{1}{2}} .$$

Thanks to the hypotheses (ii), (iii), (iv) and (v), we have:

$$\begin{aligned}
\int_z p_\theta^\alpha(z) |\ln p_\theta(z)| dz &\leq \sup_{\theta \in K} |\psi(\theta)| \cdot \sup_{\theta \in K} \int_z p_\theta^\alpha(z) dz \\
&\quad + \sup_{\theta \in K} \|\phi(\theta)\| \cdot \sum_u \left(\sup_{\theta \in K} \int_z S_u^2(z) p_\theta^\alpha(z) \right)^{\frac{1}{2}} \cdot \left(\sup_{\theta \in K} \int_z p_\theta^\alpha(z) \right)^{\frac{1}{2}} \\
&=: C(\alpha) \\
&< \infty.
\end{aligned}$$

The upper bound $C(\alpha)$ in the previous inequality is independent of θ and z but still dependant of the exponent α . However, since $\bar{B}(1, \epsilon)$ is closed ball, hypotheses (iv) and (v) can be rephrased as:

$$\begin{aligned}
(iv) \quad &\sup_{\alpha \in \bar{B}(1, \epsilon)} \sup_{\theta \in K} \int_z p_\theta^\alpha(z) dz < \infty, \\
(v) \quad &\forall u, \sup_{\alpha \in \bar{B}(1, \epsilon)} \sup_{\theta \in K} \int_z S_u^2(z) p_\theta^\alpha(z) dz < \infty.
\end{aligned}$$

Hence we can actually take the supremum in α as well:

$$\begin{aligned}
\int_z p_\theta^\alpha(z) |\ln p_\theta(z)| dz &\leq \sup_{\theta \in K} |\psi(\theta)| \cdot \sup_{\alpha \in \bar{B}(1, \epsilon)} \sup_{\theta \in K} \int_z p_\theta^\alpha(z) dz \\
&\quad + \sup_{\theta \in K} \|\phi(\theta)\| \cdot \sum_u \left(\sup_{\alpha \in \bar{B}(1, \epsilon)} \sup_{\theta \in K} \int_z S_u^2(z) p_\theta^\alpha(z) \right)^{\frac{1}{2}} \cdot \left(\sup_{\alpha \in \bar{B}(1, \epsilon)} \sup_{\theta \in K} \int_z p_\theta^\alpha(z) \right)^{\frac{1}{2}} \\
&=: C' \\
&< \infty.
\end{aligned}$$

This new upper bound C' is independent of α .

Since $T_n \mapsto 1$, then $\exists N \in \mathbb{N}, \forall n \geq N, \frac{1}{T_n} \in \bar{B}(1, \epsilon)$. Hence for $n \geq N$, we can apply the previous inequation to either $\alpha = 1$ or $\alpha = \frac{1}{T_n}$. Which gives us that

$\int_z p_\theta(z) |\ln p_\theta(z)|, \int_z p_\theta^{\frac{1}{T_n}}(z) |\ln p_\theta(z)|$ and their supremum in θ are all finite, all of them upper bounded by C' .

In the end, when $n \geq N$, we have the control $\sup_{\theta \in K} |\int_z p \ln p e^a| < C'$.

The next term to control is $\frac{1}{(1+b)^2}$. Since $b \in [0, (\frac{1}{T} - 1) \int_z p \ln p e^a]$, then $|b| \leq (\frac{1}{T} - 1) \sup_{\theta \in K} \int_z p \ln p e^a$. We already established that for all $n \geq N$, $\sup_{\theta \in K} |\int_z p \ln p e^a| \leq C' < \infty$, hence $\sup_{\theta \in K} |b(\theta, T_n)| \xrightarrow{T_n \rightarrow 1} 0$. In particular, $\exists N' \in \mathbb{N}, \forall n \geq N', \forall \theta \in K$ we

have $|b(\theta, T_n)| \leq \frac{1}{2}$. In that case:

$$\begin{aligned}
(1+b)^2 &> (1-|b|)^2 \geq \frac{1}{4} \\
\frac{1}{(1+b)^2} &< \frac{1}{(1-|b|)^2} \leq 4.
\end{aligned}$$

In the end, when $n \geq \max(N, N')$, for any $\theta \in K$:

$$\begin{aligned}
A(\theta, T_n) &\leq 2 + 2 \left(\frac{1}{T_n} - 1 \right)^2 \left(\frac{\int_z p \ln p e^a}{(1+b)^2} \right)^2 \\
&\leq 2 + 32 \left(\frac{1}{T_n} - 1 \right)^2 \left(\sup_{\theta \in K} \int_z p \ln p e^a \right)^2 \\
&\leq 2 + 32 \left(\frac{1}{T_n} - 1 \right)^2 C'^2 \\
&\leq 2 + 32 \epsilon^2 C'^2 \\
&=: C_1.
\end{aligned}$$

This upper bound does not depend on θ anymore and the part in T_n simply converges towards 0 when $T_n \rightarrow 1$.

Treating the term $B(\theta, T_n) = \left(\frac{\int_z p \ln p e^a}{(1+b)^2} \right)^2 \leq 16 \left(\sup_{\theta \in K} \int_z p \ln p e^a \right)^2 \leq 16 C'^2 =: C_2$ is immediate after having dealt with $A(\theta, T_n)$.

We now treat the term $\int_z p e^{2a} \ln^2 p$ in the exact same fashion as we did $A(\theta, T_n)$:

$$\begin{aligned}
p \ln p e^a &\in \left[p \ln p, p^{\frac{1}{T}} \ln p \right] \\
\Rightarrow p (\ln p e^a)^2 &\in \left[p \ln^2 p, p^{\frac{2}{T}-1} \ln^2 p \right] \\
\Rightarrow p (\ln p e^a)^2 &\leq \max(p \ln^2 p, p^{\frac{2}{T}-1} \ln^2 p).
\end{aligned}$$

We control those two terms as previously. First we apply Lemma 1 (its first result this time) with $\alpha \in \bar{B}(1, \epsilon)$.

$$\int_z p_\theta^\alpha(z) \ln^2 p_\theta(z) dz \leq 2 \psi(\theta)^2 \int_z p_\theta^\alpha(z) dz + 2 \|\phi(\theta)\|^2 \cdot \sum_u \int_z S_u^2(z) p_\theta^\alpha(z).$$

Thanks to the hypothesis (ii), (iii), (iv) and (v), we can once again take the supremum of the bound over $\theta \in K$, then over $\alpha \in \bar{B}(1, \epsilon)$ and conserve finite quantities:

$$\begin{aligned}
\int_z p_\theta^\alpha(z) \ln^2 p_\theta(z) dz &\leq 2 \sup_{\theta \in K} \psi(\theta)^2 \cdot \sup_{\alpha \in \bar{B}(1, \epsilon)} \sup_{\theta \in K} \int_z p_\theta^\alpha(z) dz \\
&\quad + 2 \sup_{\theta \in K} \|\phi(\theta)\|^2 \cdot \sum_u \sup_{\alpha \in \bar{B}(1, \epsilon)} \sup_{\theta \in K} \int_z S_u^2(z) p_\theta^\alpha(z) \\
&=: C_3 \\
&< \infty.
\end{aligned}$$

The previous result is true for $\alpha = 1$, and since once again $\exists N'', \forall n \geq N'', \frac{2}{T_n} - 1 \in \bar{B}(1, \epsilon) \cap \mathbb{R}_+^*$, it is also true for $\alpha = \frac{2}{T_n} - 1$ when n is large enough. C_3 is independent of z, θ and T_n .

In the end $\forall n \geq N'', \int_z p e^{2a} \ln^2 p \leq C_3 < \infty$.

We replace the three terms $A(\theta, T_n)$, $B(\theta, T_n)$ and $\int_z p e^{2a \ln^2 p}$ by their upper bounds in the inequality (11). When $n \geq \max(N, N', N'')$:

$$\int_z \frac{1}{p} \left(\frac{p^{\frac{1}{T}}}{\int_z p^{\frac{1}{T}}} - p \right)^2 \leq 2 \left(\frac{1}{T_n} - 1 \right)^2 C_1 C_3 + 2 \left(\frac{1}{T_n} - 1 \right)^2 C_2.$$

Which converges towards 0 when $T_n \rightarrow 1$, i.e. when $n \rightarrow \infty$. This concludes the proof of the lemma.

2.2.3 Verifying the conditions of Lemma 2

Now that the lemmas are proven, all that remains is to apply Lemma 2.

(i) We have $T_n \in \mathbb{R}_+^* \xrightarrow[n \rightarrow \infty]{} 1$ by hypothesis.

(ii) and (iii) $\sup_{\theta \in K} \psi(\theta) < \infty$ and $\sup_{\theta \in K} \|\phi(\theta)\| < \infty$ are implied by the fact that $\psi(\theta) = \psi'(\theta) - \log g(\theta)$ and $\phi(\theta)$ are continuous

(iv) and (v) Are also hypothesis of the theorem.
Hence we can apply Lemma 2. This means that:

$$\sup_{\theta \in K} \int_z \left(\frac{\tilde{p}_{\theta, n}(z)}{p_{\theta}(z)} - 1 \right)^2 p_{\theta}(z) dz \xrightarrow[n \rightarrow \infty]{} 0.$$

With this last condition verified, we can apply Theorem ?? . Which concludes the proof.

3 Experiments on tmp-EM with Mixtures of Gaussian

In this section, we present more detailed experiments analysing the tempered EM and comparing it to the regular EM. As in the main paper, we focus on likelihood maximisation within the Gaussian Mixture Model. From the optimisation point of view, we demonstrate that tmp-EM does not fall in the first local maximum like EM does but instead consistently finds better one. From the machine learning point of view, we illustrate how tmp-EM is able to better identify the real GMM parameters even when they are ambiguous and when the initialisation is voluntarily tricky.

The only constraints on the temperature profile is that $T_n \rightarrow 1$ and $T_n > 0$. We use two different temperature profiles. First, a decreasing exponential: $T_n = 1 + (T_0 - 1) \exp(-r.n)$. We call it the "simple" profile, it works most of the time. Second, we examine the capabilities of a profile with oscillations in addition to the main decreasing trend. These oscillations are meant to momentarily increase the convergence speed to "lock-in" some of the most obviously good decisions of the algorithm, before re-increasing the temperature and continuing the exploration on the other, more ambiguous parameters. Those two regimes are alternated in succession with gradually smaller oscillations, resulting in a multi-scale procedure

that "locks-in" gradually harder decisions. The formula is taken from [1]: $T_n = th(\frac{n}{2r}) + (T_0 - b\frac{2\sqrt{2}}{3\pi})a^{n/r} + b\text{sinc}(\frac{3\pi}{4} + \frac{n}{r})$. The profile used, as well as the values of the hyper-parameters are specified for each experiment. The hyper parameters are chosen by grid-search.

For the sake of comparison, the following Experiment 1 and 2 are similar to the experiments of [1] on the tmp-SAEM.

3.1 Experiment 1: 6 clusters

We start by demonstrating the superior performance of the tempered EM algorithm on an example mixture of $K = 6$ gaussians in dimension $p = 2$. The real parameters can be visualised on Figure 1, where the real centroids are represented by black crosses and confidence ellipses help visualise the real covariance matrices. In addition, 500 points were simulated in order to illustrate, among other things, the weights of each class. To quantify the ability of each EM method to increase

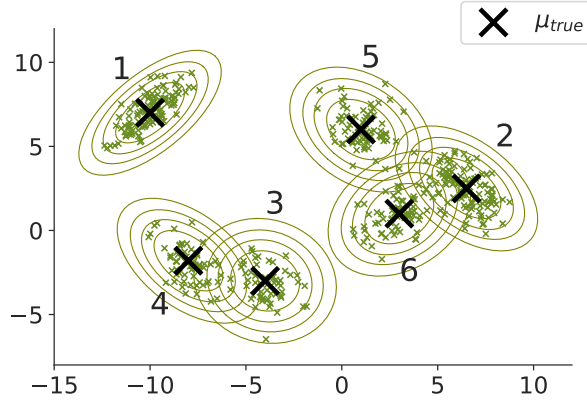


Fig. 1 500 sample points from a Mixture of Gaussians with 6 classes. The true centroid of each Gaussian are depicted by black crosses, and their true covariance matrices are represented by the confidence ellipses of level 0.8, 0.99 and 0.999 around the centre.

the likelihood and recover the true parameters, we generate from this model 20 different datasets with $n = 500$ observations. For each of these datasets, we make 200 EM runs, all of them starting from a different random initialisation. To initialise the mixture parameters, we select uniformly 6 data points to act as centroids. In each run, EM and tmp-EM start with the same initialisation. The number K of clusters is known by the algorithms. For this experiment, the simple tempering profile is used with parameters $T_0 = 50$ and $r = 2$.

3.1.1 Illustrative

First, we observe on the left of Figure 2, one example of the final states of the EM algorithm. The observations can be seen in green, the initial centroids are

represented by blue crosses, and the parameters $\{\hat{\mu}_k\}_{k=1}^K$ and $\{\hat{\Sigma}_k\}_{k=1}^K$ estimated by the EM are represented in orange. In this EM run, one of the estimated clusters became degenerated and, as counterpart, two different real clusters were fused as one by the method. On the right of Figure 2, we observe the final state of the tmp-EM on the same dataset, from the same initialisation. This time all the clusters were properly identified.

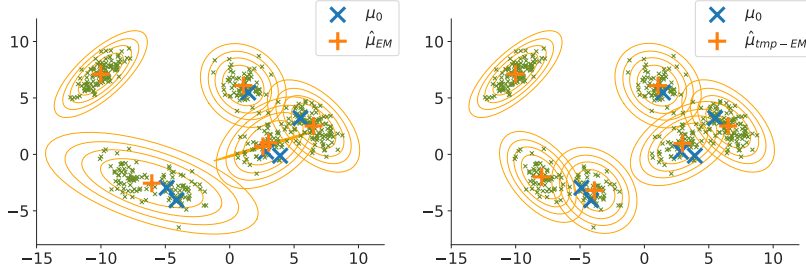


Fig. 2 EM and tmp-EM final states on the same simulation with the same initialisation. tmp-EM positioned correctly the estimated centroids, whereas the regular EM made no distinction between the two bottom classes and ended up with a degenerate class instead.

3.1.2 Quantitative

To demonstrate the improvements made by tempering, we present aggregated quantitative results over all the simulated datasets and random initialisations.

Likelihood maximisation EM and tmp-EM are optimisation methods whose target function is the likelihood of the estimated mixture parameters. We represent on Figure 3 the empirical distribution of the negative log-likelihoods reached at the end of the two methods, EM in blue, tmp-EM in orange. On those boxplots, the coloured "box" at the centre contains 50% of the distribution, hence it is delimited by the 0.25 and 0.75 quantiles. The median of the distribution is represented by an horizontal black line inside the box. The space between the whiskers on the other end, contain 90% of the distribution, its limits are the 0.05 and 0.95 quantiles. The table provides the numeric values of these statistics.

We note that the negative log-likelihood reached by tmp-EM is lower on average (higher likelihood) than what EM obtains. Moreover, tmp-EM also has a lower variance, its standard deviation being approximately half of the std of EM. More generally, we observe that the distribution of the final loss of tmp-EM is both shifted towards the lower values and less variable. In particular, each of the followed quantiles are lower for tmp-EM, and both the difference Q95-Q5 (space between whiskers) and Q75-Q25 (size of the box) are lower for tmp-EM. This illustrates that it obtains better, more consistent results on our synthetic example.

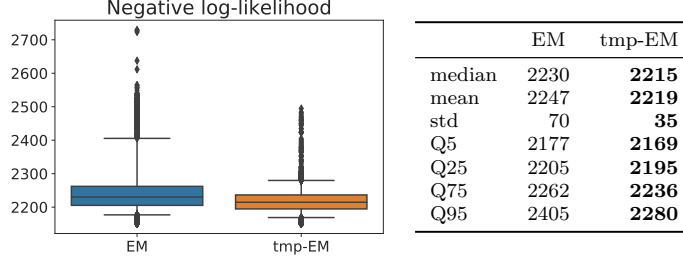


Fig. 3 Empirical distribution of the negative log-likelihood reached by the EM algorithms. EM is blue and tmp-EM in orange. The boxplot allow us to identify the quantiles 0.05, 0.25, 0.5, 0.75 and 0.95 of each distribution, as well as the outliers. Their numeric values can be found in the table, the better ones being in **bold**. tmp-EM is better overall.

Parameter recovery The EM algorithm is an optimisation procedure. Stricto sensu, the optimised metric - the likelihood - should be the only criterion for success. However, in the case of the Mixture of Gaussians, the underlying Machine Learning stakes are always very visible. Hence we dedicate time to assess the relative success parameter recovery of EM and tmp-EM.

The quality of parameter recovery is always dependent on the number of observation. The larger n , the more the likelihood will describe an actual ad-equation with the real parameters behind the simulation. Additionally, as n grows, the situation becomes less and less ambiguous, until all methods yield either the exact same, or at least very similar solutions, with all of them being fairly close to the truth. All of our simulation are done with $n = 500$ data points. Not a very large number, but since the lowest weight of our $K = 6$ classes is around 0.09, it is sufficient for all the classes to be guaranteed to contain several points. The three families of parameters in a GMM are the weights $\{\pi_k\}_{k=1}^K$, the averages (centroids positions) $\{\mu_k\}_{k=1}^K$ and the covariance matrices $\{\Sigma_k\}_{k=1}^K$ of the K classes. We evaluate the error made on μ with the relative different in squared norm 2: $\frac{\|\hat{\mu}_k - \mu_k\|_2^2}{\|\mu_k\|_2^2}$. For Σ , we compute the KL divergence between the real matrices and the estimates $KL(\Sigma_k, \hat{\Sigma}_k) = \frac{1}{2} \left(\ln \left| \frac{\Theta_k}{\hat{\Theta}_k} \right| + \text{tr}(\Sigma_k \hat{\Theta}_k) - p \right)$, with $\Theta := \Sigma^{-1}$ for all those matrices.

Finally, the analysis on π is harder to interpret and less interesting, but reveals the same trend, with lower errors for the tempering.

The error on the averages μ_k is usually the most informative and easy to interpret metric, quantifying how well each methods position the class centres. Figure 4 and Table 1 represent the distribution of the relative error $\frac{\|\hat{\mu}_k - \mu_k\|_2^2}{\|\mu_k\|_2^2}$. The results of tmp-EM are much better with average and median errors often being orders of magnitude below the errors of EM, with similar or lower variance. The other quantiles of the tmp-EM distribution are also either equivalent to or order of magnitudes below the corresponding EM quantiles. The largest errors happen on Class 3 and 6, two of the ambiguous ones, but are always noticeably smaller and less variable with the tempering.

The KL divergences $KL(\Sigma_k, \hat{\Sigma}_k)$ assess whether each the covariances Σ_k of each class are properly replicated. Note that since the computation of the KL divergence

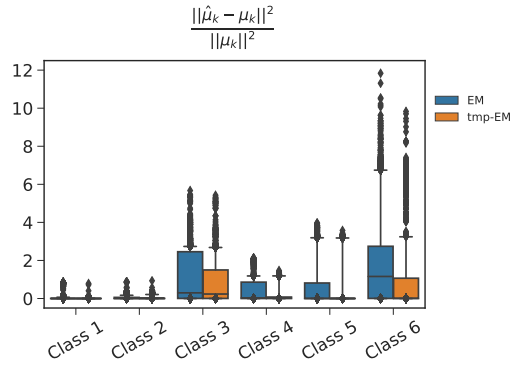


Fig. 4 Empirical distribution of the relative error in squared norm 2 $\frac{\|\hat{\mu}_k - \mu_k\|_2^2}{\|\mu_k\|_2^2}$ between the real centroid positions in μ and the estimations by the EM algorithms.

Table 1 Quantiles and other statistics describing the empirical distribution of the relative error in squared norm 2 $\frac{\|\hat{\mu}_k - \mu_k\|_2^2}{\|\mu_k\|_2^2}$ between the real centroid positions in μ and the estimations by the EM algorithms. The error of tmp-EM is always closer to 0 with lower variance (with the exception of class 2 where the variance is similar).

Cl.		mean	std	Q5	Q25	Q50	Q75	Q95
1	EM	0.024	0.119	6.10^{-6}	6.10^{-5}	2.10^{-4}	0.002	0.065
	tmp-EM	0.002	0.014	6.10^{-6}	4.10^{-5}	1.10^{-4}	4.10^{-4}	0.005
2	EM	0.038	0.066	5.10^{-5}	2.10^{-4}	0.001	0.057	0.169
	tmp-EM	0.032	0.070	5.10^{-5}	2.10^{-4}	5.10^{-4}	0.013	0.210
3	EM	0.971	1.153	4.10^{-4}	0.004	0.297	2.467	2.736
	tmp-EM	0.743	1.072	3.10^{-4}	0.003	0.235	1.500	2.681
4	EM	0.310	0.487	7.10^{-5}	8.10^{-4}	0.031	0.859	1.158
	tmp-EM	0.287	0.476	3.10^{-5}	5.10^{-4}	0.025	0.076	1.188
5	EM	0.735	1.248	8.10^{-5}	5.10^{-4}	0.002	0.814	3.191
	tmp-EM	0.432	1.054	6.10^{-5}	4.10^{-4}	7.10^{-4}	0.002	3.180
6	EM	1.940	2.828	7.10^{-4}	0.005	1.158	2.743	6.744
	tmp-EM	0.807	1.735	4.10^{-4}	0.002	0.010	1.066	3.243

involves the matrix inverse $\hat{\Theta}_k = \hat{\Sigma}_k^{-1}$, the outliers cases where a class vanishes in an EM have to be removed: they correspond to pathological, non invertible matrices. Figure 5 and Table 2 describe the distribution of the KL divergence. The Figure is cropped and does not show some of the very rare, most upper outliers (less than 1%). Overall, the results are similar to what we get on μ : in terms of average KL and median KL, tmp-EM is better than EM, being either similar on some classes and much better on others. Its standard deviation is also lower - sometimes by one order of magnitude - on all classes except Class 4. The other quantiles are also overall better, with one exception on Q95 of class 4.

Conclusion We saw that tmp-EM achieved better average and median results with lower variances both on likelihood maximisation and parameter recovery for every

Table 2 Quantiles and other statistics describing the empirical distribution of the KL divergence $KL(\Sigma_k, \hat{\Sigma}_k)$ between each covariance matrix estimated by the EMs and the real covariance matrices Σ . On every class but the 4th, the deviation of tmp-EM is closer to 0 with lower or similar variance.

Cl.		mean	std	Q5	Q25	Q50	Q75	Q95
1	EM	2.741	39.879	0.003	0.009	0.017	0.136	3.222
	tmp-EM	0.845	8.683	0.003	0.008	0.013	0.055	1.745
2	EM	0.852	9.006	0.004	0.015	0.042	0.636	1.015
	tmp-EM	0.412	9.072	0.004	0.011	0.027	0.34	0.782
3	EM	1.185	14.636	0.015	0.078	0.183	0.414	1.742
	tmp-EM	0.648	4.435	0.014	0.066	0.174	0.408	1.331
4	EM	2.008	13.156	0.008	0.043	0.386	1.034	4.553
	tmp-EM	2.998	20.1	0.006	0.028	0.374	0.637	5.468
5	EM	1.772	12.175	0.005	0.015	0.035	0.664	5.813
	tmp-EM	0.791	7.088	0.005	0.011	0.026	0.058	2.57
6	EM	2.909	59.913	0.012	0.045	0.195	0.676	4.371
	tmp-EM	2.072	25.898	0.008	0.023	0.062	0.34	2.883

Table 3 Synthetic table focusing solely on the average and standard deviation (in parenthesis) of the losses and parameter reconstruction errors made by EM and tmp-EM. We note that the likelihood reached is higher with lower variance, and similarly, the parameter metrics on almost every class are better with lower variance for tmp-EM.

Metric	class	EM	tmp-EM
$-\ln p_{\hat{\theta}}$		2 247.08 (69.62)	2 218.80 (35.21)
$\frac{\ln p_{\theta_0} - \ln p_{\hat{\theta}}}{\ln p_{\theta_0}}$		0.12 (0.04)	0.13 (0.04)
$\frac{\hat{\pi}_k - \pi_k}{\pi_k}$	1	-0.19 (0.36)	-0.17 (0.29)
	2	0.11 (0.57)	0.04 (0.33)
	3	0.56 (0.81)	0.45 (0.83)
	4	0.10 (0.57)	0.10 (0.43)
	5	-0.08 (0.48)	-0.02 (0.31)
	6	-0.20 (0.43)	-0.13 (0.40)
$\frac{\ \hat{\mu}_k - \mu_k\ ^2}{\ \mu_k\ ^2}$	1	0.02 (0.12)	2.10⁻³ (0.01)
	2	0.04 (0.07)	0.03 (0.07)
	3	0.97 (1.15)	0.74 (1.07)
	4	0.31 (0.49)	0.29 (0.48)
	5	0.73 (1.25)	0.43 (1.05)
	6	1.94 (2.83)	0.81 (1.74)
$KL(\Sigma, \hat{\Sigma})$	1	2.74 (39.88)	0.84 (8.68)
	2	0.85 (9.01)	0.41 (9.07)
	3	1.18 (14.64)	0.65 (4.44)
	4	2.01 (13.16)	3.00 (20.10)
	5	1.77 (12.17)	0.79 (7.09)
	6	2.91 (59.91)	2.07 (25.90)

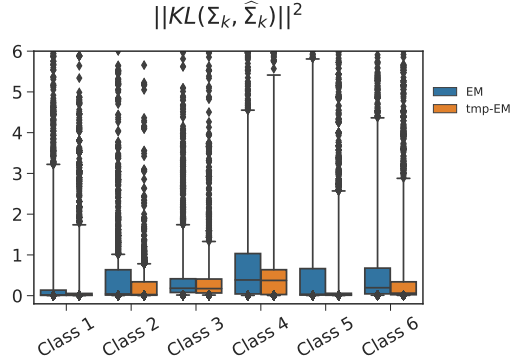


Fig. 5 Empirical distribution of the KL divergence $KL(\Sigma_k, \hat{\Sigma}_k)$ between each covariance matrix estimated by the EMs and the real covariance matrices Σ .

Class (with very rare exceptions). A more global look at the overall distributions confirms this trend: the error of tmp-EM are more centred on 0 with less spread than EM. This indicates that the tempering allows the EM algorithm to avoid falling into the first local maximum available and consistently find better ones. From the Machine Learning point of view, we highlighted that with our GMM parameters and $n = 500$ observations, it was able to better identify the different centroids, despite their ambiguity than the regular EM procedure. Table 3 presents a comparative synthesis of the results of EM and tmp-EM.

3.2 Experiment 2: 3 clusters

In this section, we will assess the capacity of tmp-EM to escape from sub-optimal local maxima near the initialisation. The experimental protocol is the same as in the main paper. Let us recall it here. We confront the algorithm to situations where the true classes have increasingly more ambiguous positions, combined with initialisations designed to be hard to escape from. Even though we still follow the log-likelihood as a critical metric, for illustrative purposes we put more emphasis in this section on visualising whether the clusters were properly identify and following the paths in the 2D space of the estimated centroids towards their final values during the EM procedures.

The setup is the following: we have three clusters of similar shape and same weight. One is isolated and easily identifiable. The other two are next to one another, in a more ambiguous configuration. Figure 6 represents the three, gradually more ambiguous configurations.

We use two different initialisation types to reveal the behaviours of the two EMs. The first - which we call "barycenter" - puts all three initial centroids at the centre of mass of all the observed data points. However, none of the EM procedures would move from this initial state if the three GMM centroids were at the exact same position, hence we actually apply a tiny perturbation to make them all slightly distinct. The blue crosses on Figure 7 represent a typical barycenter initialisation. With this initialisation method, we assess whether the EM procedures are able to

correctly estimate the positions of the three clusters, despite the ambiguity, when starting from a fairly neutral position, providing neither direction nor misdirection. On the other hand, the second initialisation type - which we call "2v1" - is voluntarily misguiding the algorithm by positioning two centroids on the isolated right cluster and only one centroid on the side of the two ambiguous left clusters. The blue crosses on Figure 8 represent a typical 2v1 initialisation. This initialisation is intended to assess whether the methods are able to escape the potential well in which they start and make their centroids traverse the empty space between the left and right clusters to reach their rightful position. For each of the three parameter families represented on Figure 6, 1000 datasets with 500 observations each are simulated, and the two EMs are ran with both the barycenter and the 2v1 initialisation. In the case of tmp-EM, the oscillating temperature profile is used with parameters $T_0 = 5$, $r = 2$, $a = 0.6$, $b = 20$ for the barycenter initialisation, and $T_0 = 100$, $r = 1.5$, $a = 0.02$, $b = 20$ for the 2v1 initialisation. Although in the case of 2v1, the oscillations are not critical, and the simple temperature profile with $T_0 = 100$ and $r = 1.5$ works as well. We have two different sets of tempering hyper-parameters values, one for each of the two very different initialisation types. However, these values then remain the same for the three different parameter families and for every data generation within them. Underlining that the method is not excessively sensitive to the tempering parameters. The experiment with 6 clusters in Section 3.1, already demonstrated that the same hyper parameters could be kept over different initialisation (and different data generations as well) when they were made in a non-adversarial way, by drawing random initial centroids uniformly among the data points.

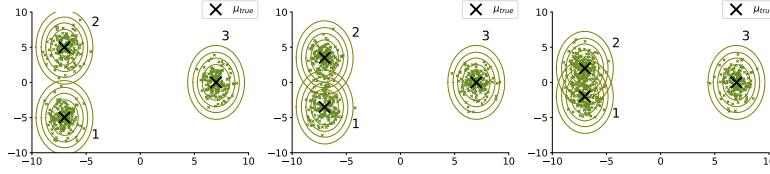


Fig. 6 500 sample points from a Mixture of Gaussians with 3 classes. The true centroid of each Gaussian are depicted by black crosses, and their true covariance matrices are represented by the confidence ellipses of level 0.8, 0.99 and 0.999 around the centre. There are three different versions of the true parameters. From left to right: the true μ_k of the two left clusters (μ_{u1} and μ_{u2}) are getting closer while everything else stays identical.

3.2.1 Illustrative

First we illustrate on unique examples how tmp-EM is able to avoid falling for the tricky initialisations we set up.

As previously stated, the focus will be less on the likelihood optimisation for these illustrative examples. Indeed, they are meant to demonstrate that tmp-EM is able to cross the gaps and put the clusters in the right place even with the disadvantageous initialisation. The more relevant metric to assess success in this task is the

error on μ (and in a lesser way, the error on Σ). One reason why the likelihood loses its ability to discriminate between failure and success in escaping the traps set by the initialisations is that there may not be a big likelihood gap between being completely wrong and mostly right. For instance placing two centroids (one of which is linked to an empty class) on the isolated left cluster and putting only one where the two ambiguously close clusters are could have a decent likelihood while being blatantly wrong.

On Figure 7, we represent the results of each EM after convergence for every of the three parameter set, when the start at the barycenter of all data points (blue crosses). The estimated means and covariance matrices of the GMM are represented by orange crosses and confidence ellipses respectively. In those examples, tmp-EM correctly identified the real clusters whereas EM put two centroids on the right, where only the isolated cluster stands, and only one on the left, where the two ambiguous clusters are. Figure 8 shows similar results, with the same conventions in the case of the "2v1" initialisation.

These different outcomes are exactly what one would expect: unlike the classical EM, tmp-EM is by design supposed to avoid the local minima close to the initialisation by taking a more exploratory stance during its first steps. To demonstrate that point, we detail in Figure 9 to 12 the paths taken by the estimated centroids by tmp-EM in those simulations. The paths of the regular EM are straightforward convergences towards their final positions, and are not represented in these supplementary materials. Figure 9 represents the paths of the three cluster centroids during the iterations of tmp-EM. The parameter family is the least ambiguous (the two left cluster are well separated) with the "barycenter" initialisation. On Figure 10, the initialisation is "2v1" instead. The two following Figures, 11 and 12, also features the initialisations "barycenter" and "2v1" respectively, but with the most ambiguous parameter set, where the two left clusters are very close to one another.

These graphs are made of several rows of figures, each row representing a step in the EM procedure. In order to make the Figures informative, the number of steps between each row is not fixed, instead the most interesting steps are represented. Convergence is always achieved within 20 to 50 steps, so there are never big differences between the step gaps anyway. The first row is always the initial stage without any EM step, and the last one is the stage after convergence. Each of the three columns corresponds to one of the three centroids estimated by the EM procedure and represents its evolution in the 2D space, from initialisation to convergence. The corresponding estimated covariance matrix is represented by confidence ellipses. For each of the centroids, the observed data points are coloured accordingly to their (un-tempered) posterior probability of belonging to the associated class at this stage of the the algorithm. Plain blue being a low probability while bright green is a high probability.

We make the following observations on the steps taken by tmp-EM: with a "barycenter" initialisation (Figure 9 and 11), the three centroids gradually converge towards their final position (which correspond to true class centres in these cases) without too much hesitation. We also note that, since the three initial points are slightly distinct, there appears to be preferences at the very beginning, with each class having different high probability points right at the initialisation stage. However

those preferences are not respected after a couple EM step, we generally see the centroids directing themselves towards different points than their initial favoured ones. This can be attributed to the tempering reshuffling the positions and preferences at the beginning. The "2v1" initialisation illustrates this phenomenon more clearly and in doing so, showcases the true power of the tempering. The very first steps after this very adversarial initialisation are not very remarkable: the single centroid on the left solidifies its position at the centre of the two ambiguous clusters, while the two centroids on the right try to share the single cluster they started in. However, very quickly this status quo is shattered and every estimated centroid jumps to a completely different position. On both Figure 10 and 12 we see the positions being completely reversed with the lonely centroid moving from the two left clusters to the isolated right one whereas the two close centroids make the inverse trip to reach the two clusters on the left. This jump is an indication that the tempering flattened the likelihood enough to allow each centroid to escape their potential wells. Effectively redoing the initialisation and allowing itself to start from more favourable positions. This behaviour is unattainable with the classical EM.

3.2.2 Quantitative

The quantitative analysis can be found in the main paper.

3.3 Experiment on real data: Wine recognition dataset

To further validate tmp-EM, we compare it once more to the unmodified EM, this time on real observations from the scikit learn [6] classification data base "Wine" [4]. This dataset contains $p = 13$ chemical measurements of $n = 178$ wines each belonging to one of $K = 3$ families. Despite being in high dimension, this dataset is known as not very challenging (the classes are separable) and useful for testing new methods. We expect the unmodified EM to perform quite well already. For tmp-EM, we use the simple decreasing temperature profile, with no oscillations, the tempering parameters are $T_0 = 100$, $r = 4$. Table 4 shows the result of 500 runs of the EMs from different random initial points. We focus on the likelihood and the error on μ_k , the other relevant metrics, not presented here, show the same tendencies. We observe, as usual, that tmp-EM reaches in average a lower negative log-likelihood with lower variance. The class centres are also better estimated. As expected, the errors made by the EM are already fairly small, however tmp-EM manages to go further and lower the errors on each class by approximately 17%, 18% and 11% respectively.

The results demonstrate that tmp-EM can improve the EM result on real data. Since this is an easy dataset, the difference is not as drastic as in the hard synthetic cases we ran the EMs by. Still, there was room to improve the EM results, and tmp-EM found those better solutions.

4 Experiments on tmp-EM with Independent Factor Analysis

In this section, we present another application of the tmp-EM with Gaussian Mixture Models, but this time as part of a more complex model. The Indepen-

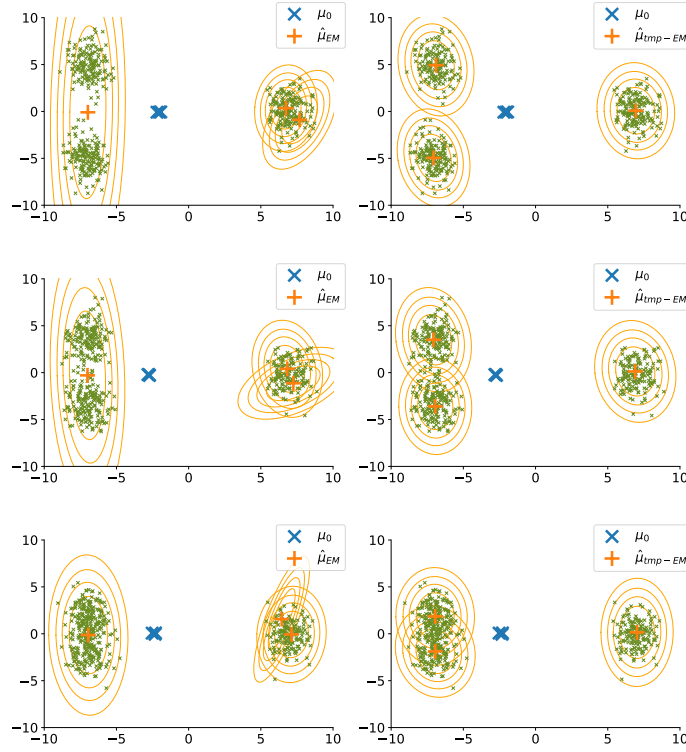


Fig. 7 Typical final positioning of the centroids by EM (left column) and tmp-EM (right column) **when the initialisation is made at the barycenter of all data points** (blue crosses). The three rows represent the three gradually more ambiguous parameter sets. Each figure represents the positions of the estimated centroids after convergence of the EM algorithms (orange cross), with their estimated covariance matrices (orange confidence ellipses). In each simulation, 500 sample points were drawn from the real GMM (small green crosses). In those example, tmp-EM managed to correctly identify the position of the three real centroids.

Table 4 Average and (standard deviation) of the EM and tmp-EM results over 500 random initialisation on the Wine recognition dataset. The classes on this dataset are easily identifiable hence the errors are low. Yet tmp-EM still improved upon the solutions of EM

metric	cl.	EM	tmp-EM
$-\ln p_{\hat{\theta}}$		2923 (77)	2905 (71)
$\frac{\ \hat{\mu}_k - \mu_k\ ^2}{\ \mu_k\ ^2}$	1	0.017 (0.030)	0.014 (0.028)
	2	0.026 (0.034)	0.021 (0.033)
	3	0.089 (0.165)	0.079 (0.156)

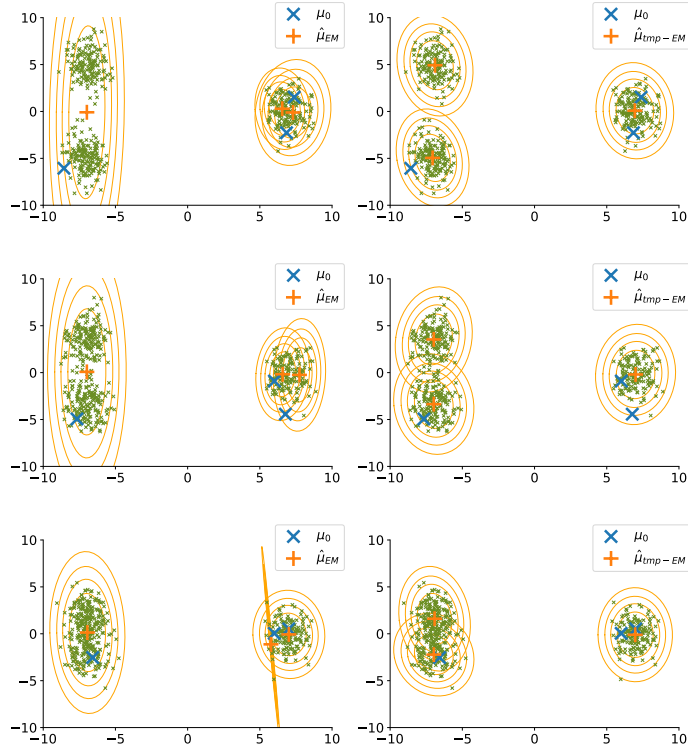


Fig. 8 Typical final positioning of the centroids by EM (left column) and tmp-EM (right column) **when the initialisation is made by selecting two points in the isolated cluster and one in the lower ambiguous cluster** (blue crosses). The three rows represent the three gradually more ambiguous parameter sets. Each figure represents the positions of the estimated centroids after convergence of the EM algorithms (orange cross), with their estimated covariance matrices (orange confidence ellipses). In each simulation, 500 sample points were drawn from the real GMM (small green crosses). In those examples, although EM kept two centroids on the isolated cluster, tmp-EM managed to correctly identify the position of the three real centroids.

dent Factor Analysis (IFA) model was introduced by [3] as an amalgam of Factor Analysis, Principal Component Analysis and Independent Component Analysis to identify and separate independent sources mixed into a single feature vector. From a practical standpoint, the mixing coefficient of each source is assumed to be drawn from a GMM, hence the EM. After estimation of the GMM parameters, the sources are recovered with an optimal non linear estimator. This is a complex model in which the EM plays a key part, works like [2] and [1] use it to assess new variants of the EM on a very practical application. The model is described as follows:

$$\forall i = 1, \dots, L', \quad y_i = \sum_{j=1}^L H_{ij} x_j + u_i.$$

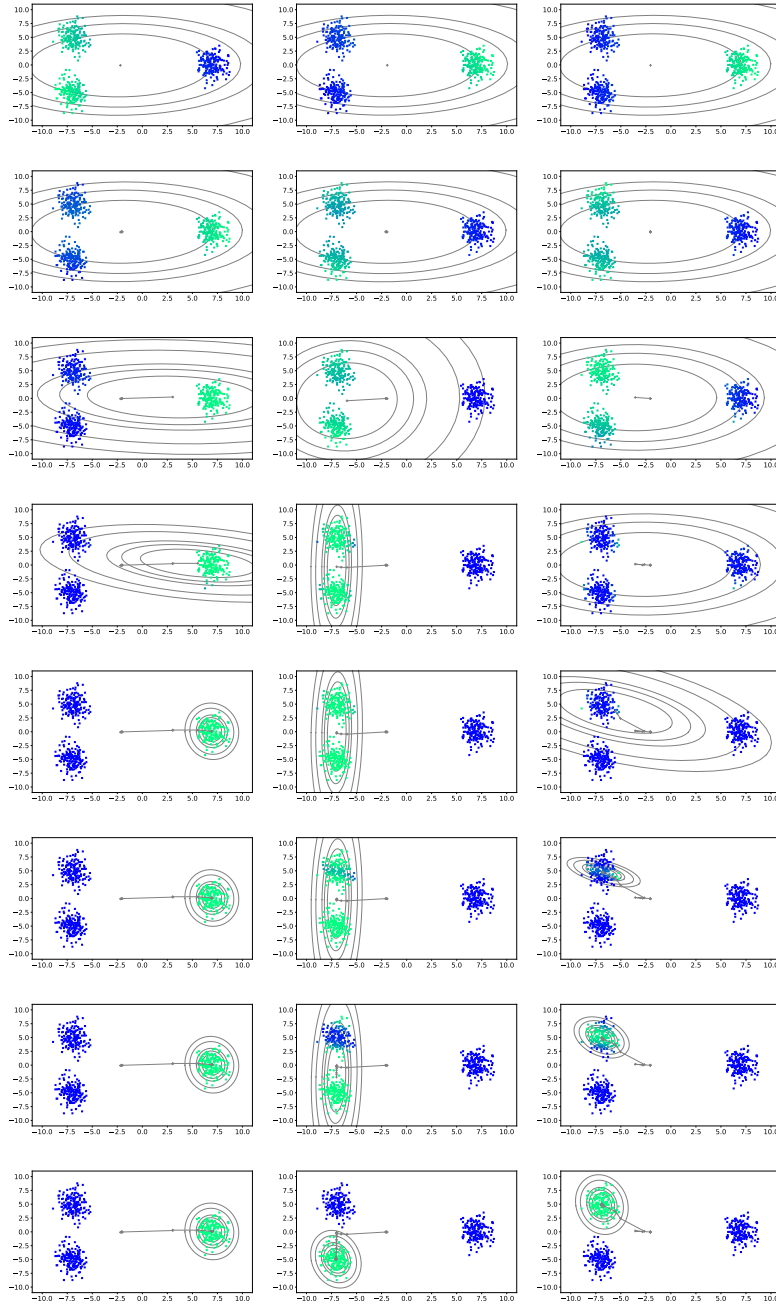


Fig. 9 Paths of the centroids for tmp-EM with the "barycenter" initialisation. Parameter set 1 (least ambiguous).

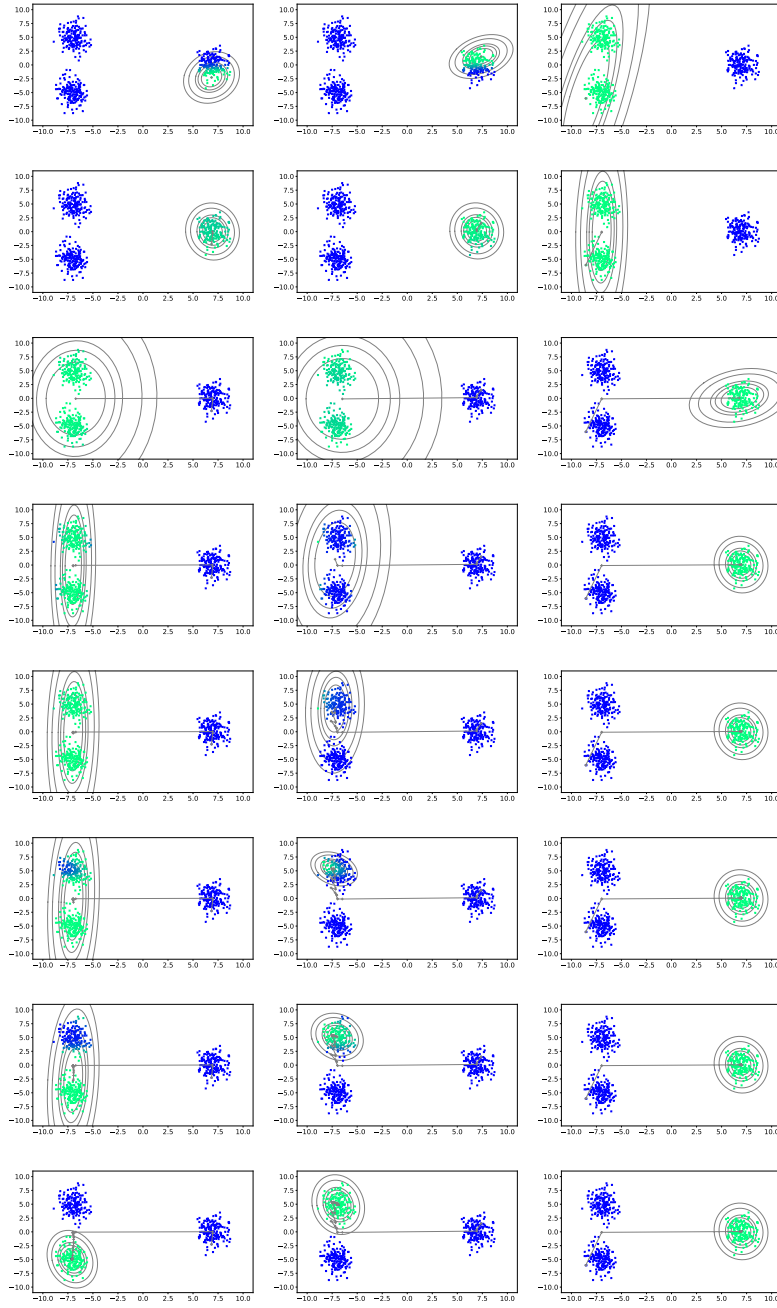


Fig. 10 Paths of the centroids for tmp-EM with the "2v1" initialisation. Parameter set 1 (least ambiguous).

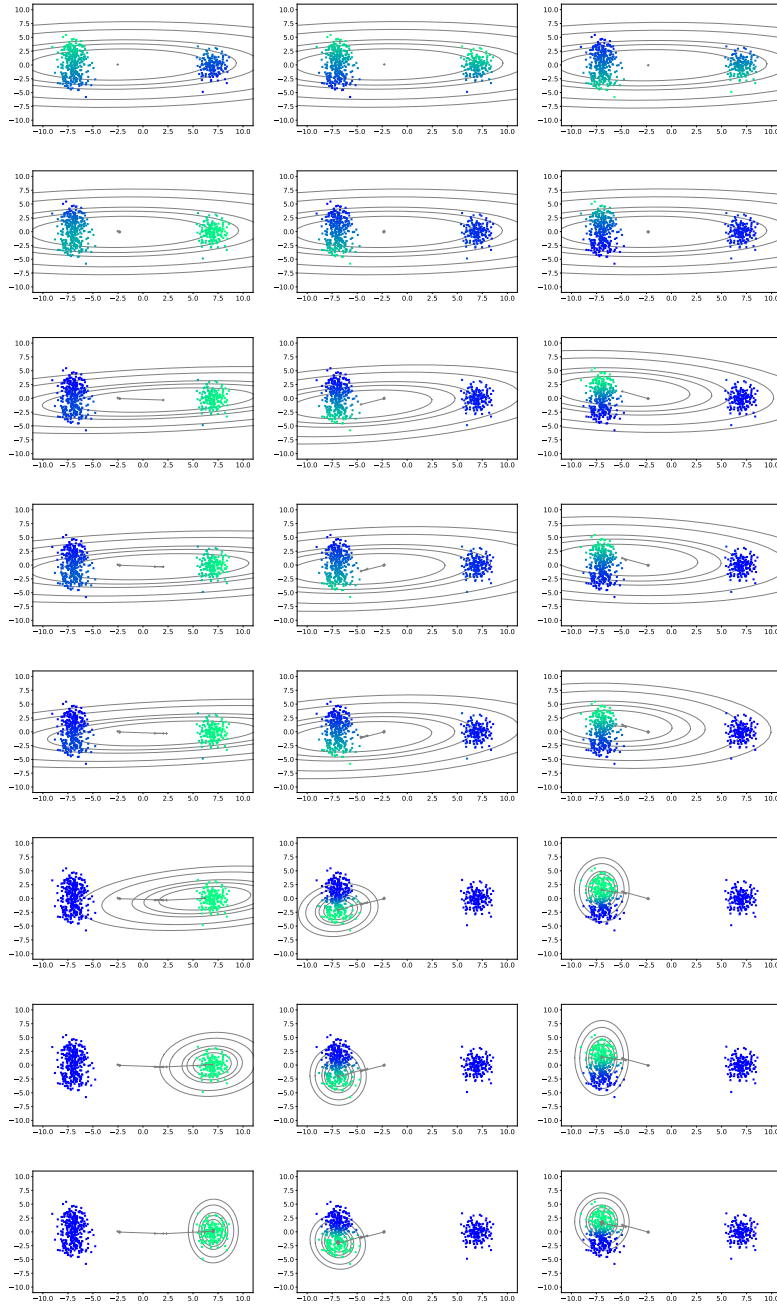


Fig. 11 Paths of the centroids for tmp-EM with the "barycenter" initialisation. Parameter set 3 (most ambiguous).

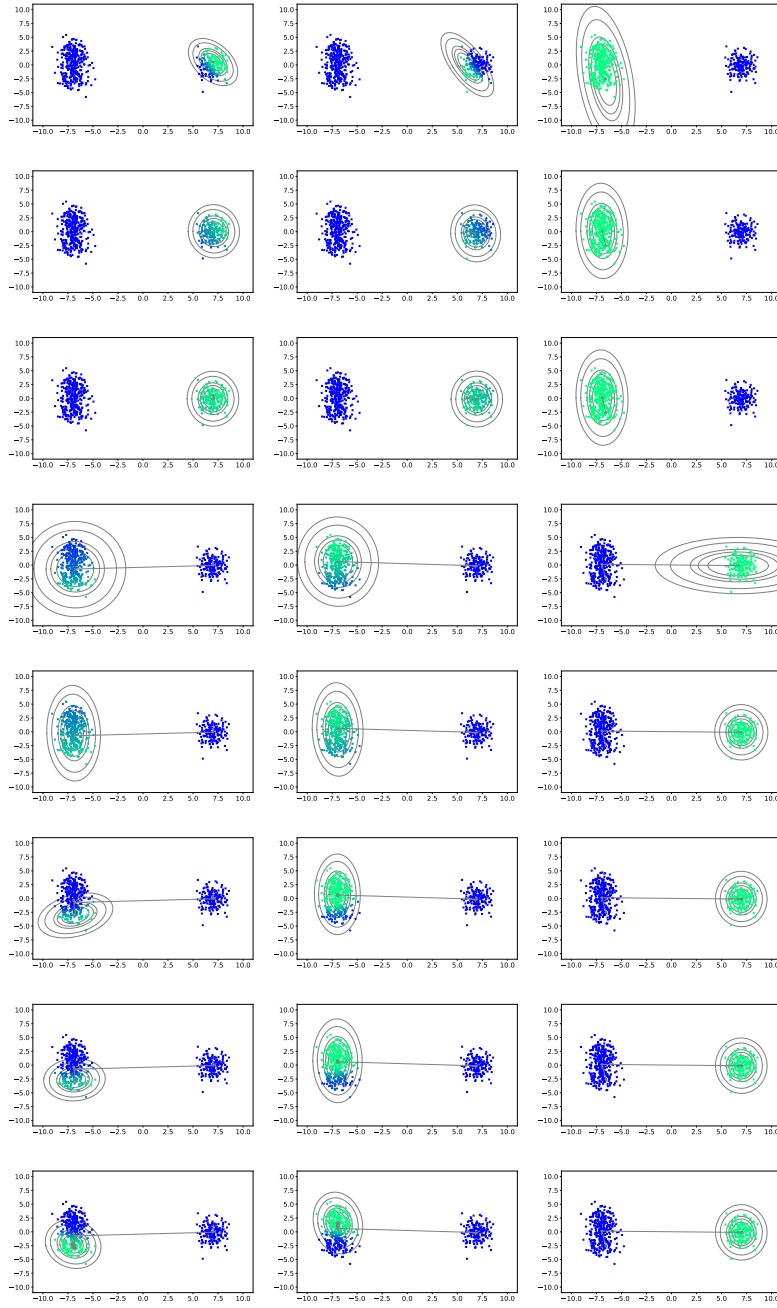


Fig. 12 Paths of the centroids for tmp-EM with the "2v1" initialisation. Parameter set 3 (most ambiguous).

Where $y \in \mathbb{R}^{L'}$ is one vector of observations, $H \in \mathbb{R}^{L' \times L}$ is the fixed matrix of the sources, $u \in \mathbb{R}^{L'}$ the vector of noise, and $x \in \mathbb{R}^L$ the random mixing coefficient. Each component x_j is assumed to be drawn from its own GMM.

An EM that converges too soon towards a local extremum has every chance to yield sub-optimal estimated sources. We demonstrate in this section that an IFA method with tmp-EM can recover sources closer to the original when they are known, and cleaner, more stable looking sources in general.

4.1 Synthetic IFA

We start with a toy example, where the true sources are two easily distinguishable images. As shown on Figure 14, one is a white square on a black background and the other is a white cross on a similar black background but positioned differently. However, once these two sources are mixed and noised, it becomes much harder to identify them with the naked eye - as illustrated by Figure 14 - and a quantitative method is required to properly separate them. To separate the sources,



Fig. 13 The two real sources of a synthetic source mixing model. They are images of size 20×20 made of a black background with a white symbol localised either on the bottom left or top right corner.

the identification model assumes that the coefficients used to mix the two sources are drawn from mixtures of gaussian. The outputs were voluntarily generated in a different way to show the generalisation capabilities of the mixture of gaussian assumption. We run an EM and a tmp-EM algorithm to estimate the parameter of those mixtures, recovering in the process an estimation of the mixing matrix H . Figure 15 illustrates the sources typically estimated by each of the two procedure. Although there is noise, tmp-EM essentially identified and corrected the sources correctly. Whereas EM did not manage to completely turn off the square symbol in the estimated sources supposedly dedicated to the cross. Figure 16 displays the quantitative results of several runs over different simulated datasets. It represents the empirical distribution of l_2 errors made on the estimation of the source matrix H by the two EMs. As illustrated by the table in Figure 16, the solutions of tmp-EM have lower mean and median.

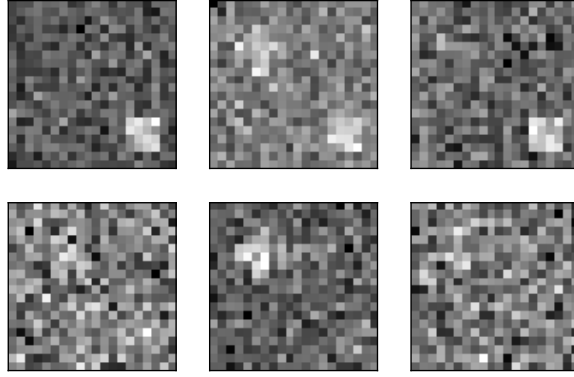


Fig. 14 6 typical observation obtained with the source mixing model. With the noise, the sources are harder to identify.

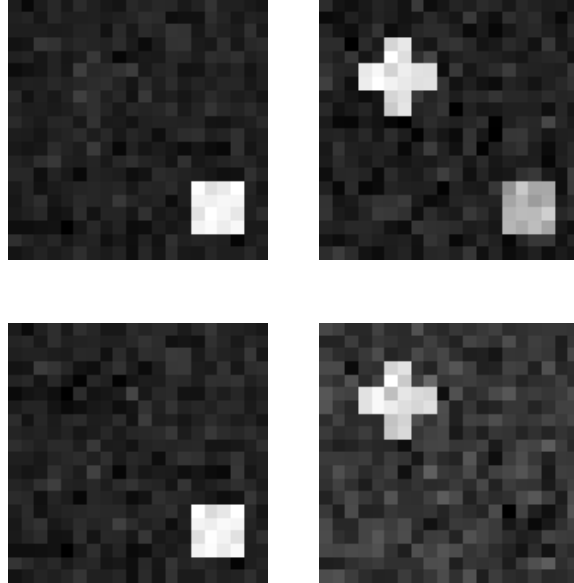


Fig. 15 Estimated sources by EM (up) and tmp-EM (down). The two real sources were correctly identify by tmp-EM, but EM did not fully separate the cross and the square.

4.2 ZIP code

We apply this IFA algorithm to the ZIP code dataset from Elements of Statistical learning. This dataset contains handwritten digits between 0 and 9. In this study, we keep only the digits 0,3, 8 (all three being ambiguously similar) and 7 (very different from the three others). We make all classes even by removing half of the 0

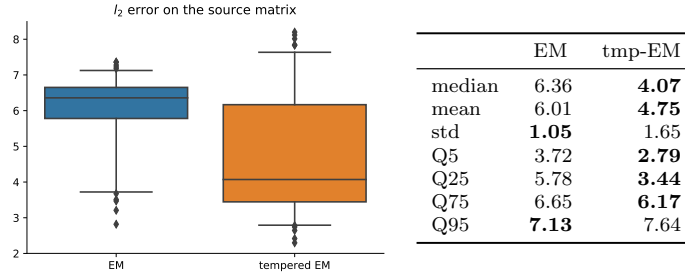


Fig. 16 Empirical distribution of the l_2 error on the source matrix H made by EM and tmp-EM. With tmp-EM, we shift the distribution towards the lower errors, with smaller average and median. The numeric values of the quantiles and other statistics can be found in the table, the better ones being in **bold**.

which are originally more numerous. When applying Independent Factor Analysis to such data, one hopes that the distinct digits will be identified as the separable sources making up the signal. We run the IFA model with a Mixture of Gaussians model with a regular and a tempered EM. In the mixing model used, each mixture is composed of two classes. The tempering was made with the oscillating profile, with hyper-parameters: $T_0 = 50$, $b = 20$, $r = 3$, $a = 0.02$.

Figure 17 displays the estimated sources by the IFA procedure with either EM or tmp-EM at their core. EM did not really identify an "8" source. Instead, its "3" is a bit ambiguously close to an "8", and the rightmost source in Figure 17 seems like an amalgamation of the four digits. Moreover, the source "7" estimated by EM is actually a mix between a "7" and a "0". On the other hand, the sources estimated by tmp-EM each correspond clearly to a different digit. There is an "8", the "7" is not fused with a "0", the "3" is sharper and more distinct from an "8" than the corresponding EM source, and even the "0" is more symmetrical with tmp-EM than with EM. Tempering the EM within the IFA algorithm allowed for a cleaner separation of the sources. One can infer that tmp-EM was able to identify and reach a better local maximum of the loss function.



Fig. 17 Estimated sources by EM (up) and tmp-EM (down). The "8" and the "7" in particular were much better identified by tmp-EM. Moreover, with tempering the "0" has a more symmetrical shape and the "3" is sharper and less ambiguous.

References

1. Allasonnière, S., Chevallier, J.: A New Class of EM Algorithms. Escaping Local Minima and Handling Intractable Sampling (2019). URL <https://hal.archives-ouvertes.fr/hal-02044722>. Working paper or preprint
2. Allasonniere, S., Younes, L., et al.: A stochastic algorithm for probabilistic independent component analysis. *The Annals of Applied Statistics* **6**(1), 125–160 (2012)
3. Attias, H.: Independent factor analysis. *Neural computation* **11**(4), 803–851 (1999)
4. Dua, D., Graff, C.: UCI machine learning repository (2017). URL <http://archive.ics.uci.edu/ml>
5. Fort, G., Moulines, E.: Convergence of the monte carlo expectation maximization for curved exponential families. *The Annals of Statistics* **31**(4), 1220–1259 (2003)
6. Pedregosa, F., Varoquaux, G., Gramfort, A., Michel, V., Thirion, B., Grisel, O., Blondel, M., Prettenhofer, P., Weiss, R., Dubourg, V., Vanderplas, J., Passos, A., Cournapeau, D., Brucher, M., Perrot, M., Duchesnay, E.: Scikit-learn: Machine learning in Python. *Journal of Machine Learning Research* **12**, 2825–2830 (2011)